(2)

DNA-TR-89-73

A SIGNAL REALIZATION DATA BASE GENERATED BY THE MULTIPLE PHASE-SCREEN METHOD

D. J. Krueger
M. O. Duff
S. M. Frasier
Mission Research Corporation
P.O. Drawer 719
Santa Barbara, CA 93102-0719

24 March 1989

Technical Report

CONTRACT No. DNA 001-87-C-0169

Approved for public release; distribution is unlimited.

THIS WORK WAS SPONSORED BY THE DEFENSE NUCLEAR AGENCY UNDER RDT&E RMC CODES B466D RB RB OP140 25904D, B466D RB RB EA104 25904D, and B466D RB RB 00140 25904D.

Prepared for
Director
Defense Nuclear Agency
Washington, DC 20305-1000

Destroy this report when it is no longer needed. Do not return to sender.

PLEASE NOTIFY THE DEFENSE NUCLEAR AGENCY, ATTN: CSTI, WASHINGTON, DC 20305-1000, IF YOUR ADDRESS IS INCORRECT, IF YOU WISH IT DELETED FROM THE DISTRIBUTION LIST, OR IF THE ADDRESSEE IS NO LONGER EMPLOYED BY YOUR ORGANIZATION.

DISTRIBUTION LIST UPDATE

This mailer is provided to enable DNA to maintain current distribution lists for reports. We would appreciate your providing the requested information.

☐ Add the individual listed to your distribution list.

☐ Delete the cited organization/individual.

☐ Change of address.

NAME: _____

ORGANIZATION: _____

OLD ADDRESS	CURRENT ADDRESS
_____	_____
_____	_____
_____	_____

TELEPHONE NUMBER: (___) _____

SUBJECT AREA(s) OF INTEREST:

_____

_____

_____

DNA OR OTHER GOVERNMENT CONTRACT NUMBER: _____

CERTIFICATION OF NEED TO KNOW BY GOVERNMENT SPONSOR (if other than DNA):

SPONSORING ORGANIZATION: _____

CONTRACTING OFFICER OR REPRESENTATIVE

SIGNATURE

CUT HERE AND RETURN

REPORT DOCUMENTATION PAGE

1a. REPORT SECURITY CLASSIFICATION UNCLASSIFIED	1b. RESTRICTIVE MARKINGS
2a. SECURITY CLASSIFICATION AUTHORITY N/A since Unclassified	3. DISTRIBUTION/AVAILABILITY OF REPORT Approved for public release; distribution is unlimited.
2b. DECLASSIFICATION/DOWNGRADING SCHEDULE N/A since Unclassified	
4. PERFORMING ORGANIZATION REPORT NUMBER(S) MRC-R-1223	5. MONITORING ORGANIZATION REPORT NUMBER(S) DNA-TR-89-73
6a. NAME OF PERFORMING ORGANIZATION Mission Research Corporation 6b. OFFICE SYMBOL (if applicable)	7a. NAME OF MONITORINNG ORGANIZATION Director Defense Nuclear Agency
6c. ADDRESS (City, State, and ZIP Code) P.O. Drawer 719 Santa Barbara, CA 93102-0719	7b. ADDRESS (City, State, and ZIP Code) Washington, DC 20305-1000
8a. NAME OF FUNDING/SPONSORING ORGANIZATION 8b. OFFICE SYMBOL (if applicable) RAAE/Wittwer	9. PROCUREMENT INSTRUMENT IDENTIFICATION NUMBER DNA 001-87-C-0169
8c. ADDRESS (City, State, and ZIP Code)	10. SOURCE OF FUNDING NUMBERS PROGRAM ELEMENT NO. 62715H; PROJECT NO. RB; TASK NO. RB; WORK UNIT ACCESSION NO DH870169

11. TITLE (Include Security Classification)
A SIGNAL REALIZATION DATA BASE GENERATED BY THE MULTIPLE PHASE-SCREEN METHOD

12. PERSONAL AUTHOR(S)
Krueger, D. J.; Duff M. O.; Frasier, S. M.

13a. TYPE OF REPORT	13b. TIME COVERED	14. DATE OF REPORT (Year, Month, Day)	15. PAGE COUNT
Technical	FROM 881215 TO 890324	890324	78

16. SUPPLEMENTARY NOTATION
This work was sponsored by the Defense Nuclear Agency under RDT&E RMC Codes B466D RB RB OP140 25904D, B466D RB RB EA104 25904D, and B466D RB RB 00140 25904D.

17. COSATI CODES		
FIELD	GROUP	SUB-GROUP
25	2	
20	14	

18. SUBJECT TERMS (Continue on reverse if necessary and identyly by block number)
Satellite Communications; Propagation Effects; MPS Signal Scintillation; Data Base.

19. ABSTRACT (Continue on reverse if necessary and identify by block number)

This report is intended to serve as supporting documentation for an accompanying magnetic tape which contains realizations of signals resulting from propagation through a striated ionosphere (parameterized as fifteen different cases of carrier frequency and electron-density variance). The signals were generated with a Multiple Phase-Screen (MPS) computer code, and the simulated cases range, in their levels of effect, from very weakly scattered cases to those where the signals display intensity profiles characteristic of Rayleigh amplitude fluctuations. This report details what is represented on the magnetic tape and provides information regarding its use. The appendices present supplementary material on the MPS technique, provide example software that may be used to read realization data, and summarize the MPS runs with plots and tables. Keywords:

20. DISTRIBUTION/AVAILABILITY OF ABSTRACT	21. ABSTRACT SECURITTY CLASSIFICATION
☐ UNCLASSIFIED/UNLIMITED ☒ SAME AS REPORT ☐ DTIC USERS	UNCLASSIFIED

22a. NAME OF RESPONSIBLE INDIVIDUAL	22b. TELEPHONE (Include Area Code)	22c. OFFICE SYMBOL
Bennie F. Maddox	(202) 325-7028	DNA/CSTI

DD FORM 1473, 84 MAR — 83 APR edition may be used until exhausted. All other editions are obsolete.

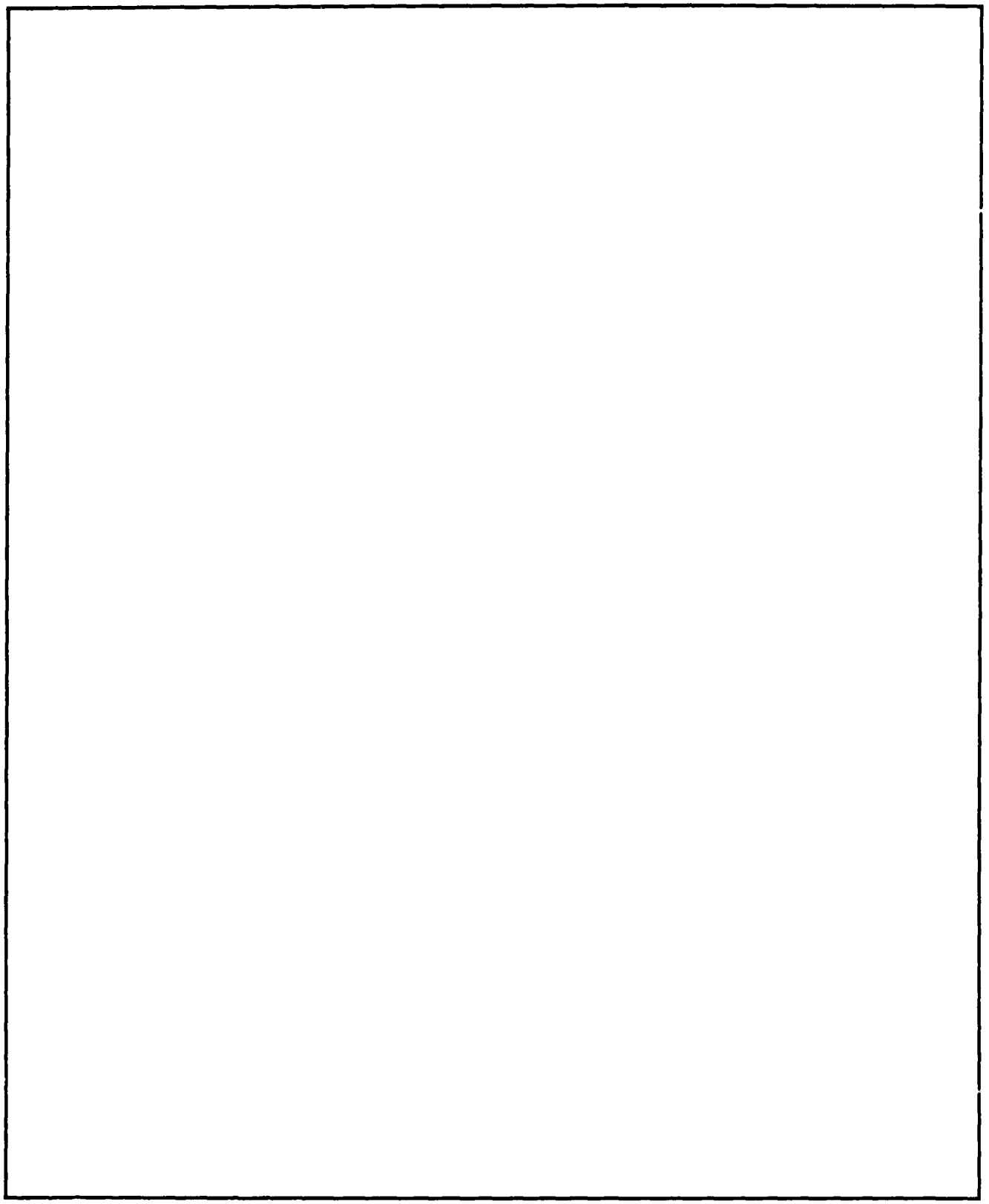

CONVERSION TABLE

Conversion factors for U.S. Customary to metric (SI) units of measurement

MULTIPLY →	BY →	TO GET
TO GET ←	BY ←	DIVIDE
angstrom	1.000000 x E -10	meters (m)
atmosphere (normal)	1.01325 x E +2	kilo pascal (kPa)
bar	1.000000 x E +2	kilo pascal (kPa)
barn	1.000000 x E -28	meter^2 (m^2)
British thermal unit (thermochemical)	1.054350 x E +3	joule (J)
calorie (thermochemical)	4.184000	joule (J)
cal (thermochemical) / cm^2	4.184000 x E -2	mega joule/m^2 (MJ/m^2)
curie	3.700000 x E +1	*giga becquerel (GBq)
degree (angle)	1.745329 x E -2	radian (rad)
degree Farenheit	$t_K = (t_F + 459.67)/1.8$	degree kelvin (K)
electron volt	1.60219 x E -19	joule (J)
erg	1.000000 x E -7	joule (J)
erg/second	1.000000 x E -7	watt (W)
foot	3.048000 x E -1	meter (m)
foot-pound-force	1.355818	joule (J)
gallon (U.S. liquid)	3.785412 x E -3	meter^3 (m^3)
inch	2.540000 x E -2	meter (m)
jerk	1.000000 x E +9	joule (J)
joule/kilogram (J/kg) (radiation dose absorbed)	1.000000	Gray (Gy)
kilotons	4.183	terajoules
kip (1000 lbf)	4.448222 x E +3	newton (N)
kip/inch^2 (ksi)	6.894757 x E +3	kilo pascal (kPa)
ktap	1.000000 x E +2	newton-second/m^2 (N-s/m^2)
micron	1.000000 x E -6	meter (m)
mil	2.540000 x E -5	meter (m)
mile (international)	1.609344 x E +3	meter (m)
ounce	2.834952 x E -2	kilogram (kg)
pound-force (lbs avoirdupois)	4.448222	newton (N)
pound-force inch	1.129848 x E -1	newton-meter (N·m)
pound-force/inch	1.751268 x E +2	newton/meter (N/m)
pound-force/foot^2	4.788026 x E -2	kilo pascal (kPa)
pound-force/inch^2 (psi)	6.894757	kilo pascal (kPa)
pound-mass (lbm avoirdupois)	4.535924 x E -1	kilogram (kg)
pound-mass-foot^2 (moment of inertia)	4.214011 x E -2	kilogram-meter^2 (kg·m^2)
pound-mass/foot^3	1.601846 x E +1	kilogram/meter^3 (kg/m^3)
rad (radiation dose absorbed)	1.000000 x E -2	**Gray (Gy)
roentgen	2.579760 x E -4	coulomb/kilogram (C/kg)
shake	1.000000 x E -8	second (s)
slug	1.459390 x E +1	kilogram (kg)
torr (mm Hg, 0° C)	1.333220 x E -1	kilo pascal (kPa)

*The becquerel (Bq) is the SI unit of radioactivity; 1 Bq = 1 event/s.
**The Gray (Gy) is the SI unit of absorbed radiation.

TABLE OF CONTENTS

Section		Page
	CONVERSION TABLE	iii
	LIST OF ILLUSTRATIONS	v
	LIST OF TABLES	vii
1	**THE MULTIPLE PHASE-SCREEN METHOD**	1
2	**THE DATA BASE**	3
	2.1 WHAT IS REPRESENTED IN THE DATA BASE.	3
	2.2 HOW TO ACCESS INFORMATION IN THE DATA BASE.	9
3	**LIST OF REFERENCES**	15

Appendices

A	**THEORETICAL OVERVIEW**	17
B	**MPS OUTPUT FILE DESCRIPTION**	23
C	**FORTRAN SUBROUTINE FOR SAMPLING REALIZATIONS**	31
D	**DISCUSSION AND DETAILED SUMMARY OF THE MPS RUNS**	35

LIST OF ILLUSTRATIONS

Figure		Page
1	MPS geometry	5
2	Plots of phase, intensity, and their respective power spectral densities for a realization with $\langle \chi^2 \rangle = .03$ (10 GHz)	7
3	Plots of phase, intensity, and their respective power spectral densities for a realization with $\langle \chi^2 \rangle = .32$ (10 GHz)	8
4	Strongly-scattered case compared to a theoretical Rayleigh signal	10
5	Theoretical slope structure in the phase PSD corresponding to the most weakly-scattered case (10 GHz)	10
6	Phase-screen representation of the ionized region	18
7	Comparison of theoretical and measured values for $\langle \chi^2 \rangle$ and ℓ_0	45
8	Representative phase, intensity, and power spectral density plots for case 4001	46
9	Representative phase, intensity, and power spectral density plots for case 4002	47
10	Representative phase, intensity, and power spectral density plots for case 4003	48
11	Representative phase, intensity, and power spectral density plots for case 4004	49
12	Representative phase, intensity, and power spectral density plots for case 4005	50
13	Representative phase, intensity, and power spectral density plots for case 4006	51
14	Representative phase, intensity, and power spectral density plots for case 4007	52
15	Representative phase, intensity, and power spectral density plots for case 4008	53

LIST OF ILLUSTRATIONS (CONCLUDED)

Figure		Page
16	Representative phase, intensity, and power spectral density plots for case 4009	54
17	Representative phase, intensity, and power spectral density plots for case 4010	55
18	Representative phase, intensity, and power spectral density plots for case 4011	56
19	Representative phase, intensity, and power spectral density plots for case 4012	57
20	Representative phase, intensity, and power spectral density plots for case 4013	58
21	Representative phase, intensity, and power spectral density plots for case 4014	59
22	Representative phase, intensity, and power spectral density plots for case 4015	60
23	Comparison of Rayleigh, Rician, and Nakagami-m PDFs and CDFs for case 4001	61
24	Comparison of Rayleigh, Rician, and Nakagami-m PDFs and CDFs for case 4002	62
25	Comparison of Rayleigh, Rician, and Nakagami-m PDFs and CDFs for case 4003	63
26	Comparison of Rayleigh, Rician, and Nakagami-m PDFs and CDFs for case 4004	64
27	Comparison of Rayleigh, Rician, and Nakagami-m PDFs and CDFs for case 4005	65

LIST OF TABLES

Table		Page
1	Summary of MPS calculations	6
2a	Description and summary of 10 GHz data base	12
2b	Description and summary of 3.16 GHz data base	13
2c	Description and summary of 1 GHz data base	14
3a	Detailed MPS realization summary of cases 4001-4005 (10 GHz) . .	39
3b	Detailed MPS realization summary of cases 4006-4010 (3.16 GHz) .	41
3c	Detailed MPS realization summary of cases 4011-4015 (1 GHz) . . .	43

SECTION 1

THE MULTIPLE PHASE-SCREEN METHOD

In the Multiple Phase-Screen method (MPS), the ionized medium is divided into a finite number of layers and each layer is represented by a thin diffracting screen (see Appendix A and References 3 and 4 for more details). MPS provides an exact solution to the parabolic wave equation describing a plane, unmodulated carrier-wave traversing this series of phase-perturbing screens. Hence MPS is "exact" in that the fidelity of its results is limited only by the extent to which the parabolic equation approximation and phase-spectrum description of the environment preserve the true dynamical and environmental characteristics of the problem.

It should be stressed that MPS calculates actual values of signal amplitude and phase (I and Q voltage levels) at the receiver plane; the method is fundamentally different from procedures that replace the ionized layer with an explicit statistical model for the received signal. In MPS, although realizations of the phase-changing screens are generated in a random manner based upon a sequence of pseudo-random numbers (consistent with the layer's phase-variance description), once these random numbers are generated, the phase-screens are completely defined and known. Similarly, the wave field propagated through the phase-screens is subject to exact calculation. However, a different sequence of pseudo-random numbers will yield a different set of phase-screen realizations and hence a different realization of the received electric field. Realizations of the received signal amplitude and phase are important results of the simulation and in turn serve as direct input to detailed receiver simulations.

MPS can handle all levels of ionospheric disturbances, from the least severe with only minor phase fluctuations to the most severe cases of frequency selective Rayleigh fading. It is in the cases of weak scattering that MPS methods prove most useful, since in these cases the signal amplitude statistics are neither Rayleigh nor Rician – their description is quite complex and cannot be accurately generated by other, more analytically-based, models that make assumptions regarding the statistical character of the signals.

Though exact, the MPS method is limited in its application by its requirement that the electric field and phase be adequately represented by values at a discrete number of grid points; that is, in order to provide a faithful description of the phase distribution and avoid angular aliasing and/or scattering, the phase-screen grid point spacing must be fine enough and the phase-screen length must be long enough. For

propagation environments parameterized by large values of phase-variance and/or small fluctuation scale-size, these requirements may call for a prohibitively large number of grid points.

Fortunately, there exist other methods for simulating strongly-scattered signals. The Antenna/Channel Impulse Response Function (ACIRF) code (see Reference 1), which implements the DNA-approved statistical generation technique, is far less computationally intensive than MPS but relies strongly on the assumption that Rayleigh statistics govern the amplitude fluctuations of the signals of interest.

Thus the MPS method is well-suited for the cases of comparatively weak scattering, where the Rayleigh assumptions upon which ACIRF is based break down, and ACIRF provides appropriate realizations for strongly-scattered Rayleigh signals, when the grid resolution requirements of MPS prove too costly computationally.

SECTION 2

THE DATA BASE

2.1 WHAT IS REPRESENTED IN THE DATA BASE.

The magnetic tape contains the results of a series of fifteen MPS runs. Each run or "case" corresponds to a specific choice for electron density variance and radiofrequency wavelength, and the output of each MPS run is a series of signal realizations – actual values of signal amplitude and phase (I and Q voltage levels) – at the receiver plane. The simulated cases fall conceptually into three distinct wavelength classes, each with its own unique set of five fluctuation levels. Within each wavelength class, the electron density variance values specified produce scintillation effects that range from weak to strong scattering:

Electron Density Variance: $[cm^{-6}]$		
Wavelength		
3 cm	9.5 cm	30 cm
2.12×10^{13}	4.26×10^{11}	9.37×10^{9}
6.72×10^{13}	1.35×10^{12}	2.96×10^{10}
2.12×10^{14}	4.26×10^{12}	9.37×10^{10}
6.72×10^{14}	1.35×10^{13}	2.96×10^{11}
2.12×10^{15}	4.26×10^{13}	9.37×10^{11}

The ionized layer through which the plane wave propagates imparts a phase-shift that is a function of distance along the horizontal axis of the layer. The variance of this phase-shift, the "phase-variance", is determined in part by the electron density variance, fluctuation scale sizes, and the layer-thickness. The MPS method replaces the entire layer by a smaller number of thin layers, and compresses the thin layers into phase-perturbing screens that preserve phase-variance.

The index of refraction fluctuations of the ionized layer are characterized by a two-component power spectral density (see Appendix A) whose parameters include:

Outer Scale Size – 10 km/rad,
Freezing Scale Size – 300 m/rad,
Inner Scale Size – 2 m/rad,
Intermediate Scale Parameter n – 1.75, and
Transition Scale Parameter n' – 2.5.

Together with

Layer Thickness for an Individual Phase Screen – 24.6 km,
Total Number of Layers – 11, and
Briggs Parkins Angle – 90 deg.,

the power spectral density of the layer (and electron density variance) determines the power spectral density of the MPS phase-screens.

The MPS simulation is also dependent upon geometry. Relevant descriptors are presented in Figure 1. There are 2^{17} grid points along the space axis for a spatial resolution of two meters.

MPS requires as input the phase-variance per screen and the wave frequency. The preceding table becomes (see Appendix A for conversion details):

Phase-Variance per Screen: [rad^2]		
Frequency		
10 GHz	3.16 GHz	1 GHz
5.63×10^1	1.13×10^1	2.49
1.78×10^2	3.59×10^1	7.85
5.63×10^2	1.13×10^2	2.49×10^1
1.78×10^3	3.59×10^2	7.85×10^1
5.63×10^3	1.13×10^3	2.49×10^2

Table 1 summarizes the resulting MPS calculations. The entries for each case are average values over ten realizations. For each frequency class, as the total phase-variance increases, the mean-squared value of the logarithm of signal amplitude, $\langle \chi^2 \rangle$, increases from .010 toward .5, the normalized intensity variance, S_4, becomes partially-saturated, and the decorrelation distance, ℓ_0, decreases.

Figures 2 and 3 are typical realization profiles. In Figure 2, a weakly-scattered case, intensity fluctuations are due to a mixture of refraction and diffraction

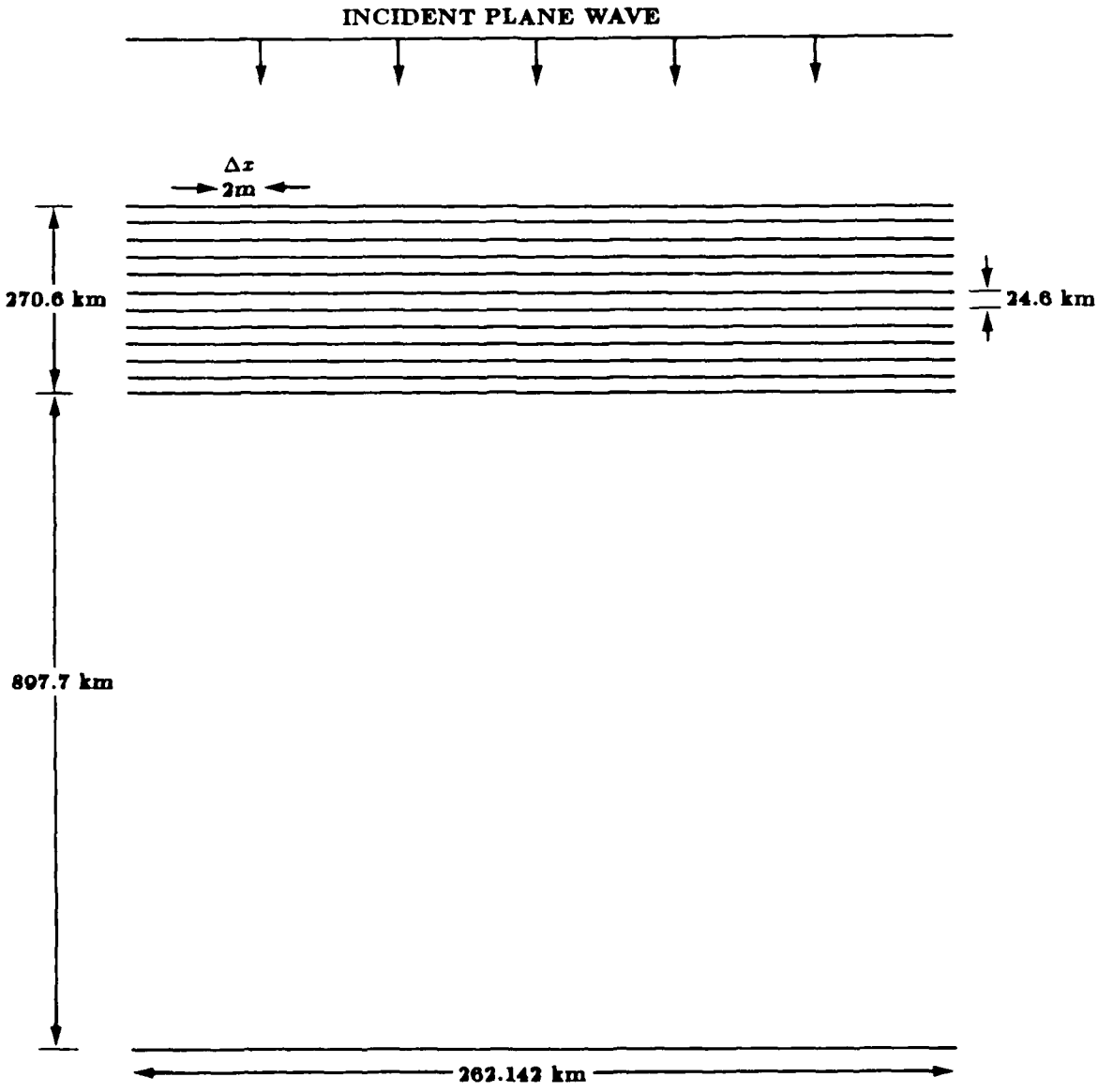

Figure 1. MPS geometry.

Table 1. Summary of MPS calculations.

Case #	Frequency	$\sigma^2_{N_e}$ Electron Density Variance [cm^{-6}]	σ^2_ϕ Total Phase Variance [rad^2]	$< \chi^2 >$	S_4	ℓ_0 [m]
4001	10 GHz	2.12E+13	6.20E+02	.00980	.201	191
4002	(λ = 3 cm)	6.72E+13	1.96E+03	.0312	.369	105
4003		2.12E+14	6.20E+03	.103	.698	58.0
4004		6.72E+14	1.96E+04	.315	1.12	32.4
4005		2.12E+15	6.20E+04	.570	1.31	18.1
4006	3.16 GHz	4.26E+11	1.25E+02	.00983	.201	457
4007	(λ = 9.5 cm)	1.35E+12	3.95E+02	.0315	.366	243
4008		4.26E+12	1.25E+03	.107	.678	132
4009		1.35E+13	3.95E+03	.327	1.08	73.1
4010		4.26E+13	1.25E+04	.559	1.24	40.7
4011	1 GHz	9.37E+09	2.73E+01	.00986	.200	1120
4012	(λ = 30 cm)	2.96E+10	8.64E+01	.0316	.361	563
4013		9.37E+10	2.73E+02	.109	.648	296
4014		2.96E+11	8.64E+02	.331	1.01	160
4015		9.37E+11	2.7E+03	.548	1.18	88.3

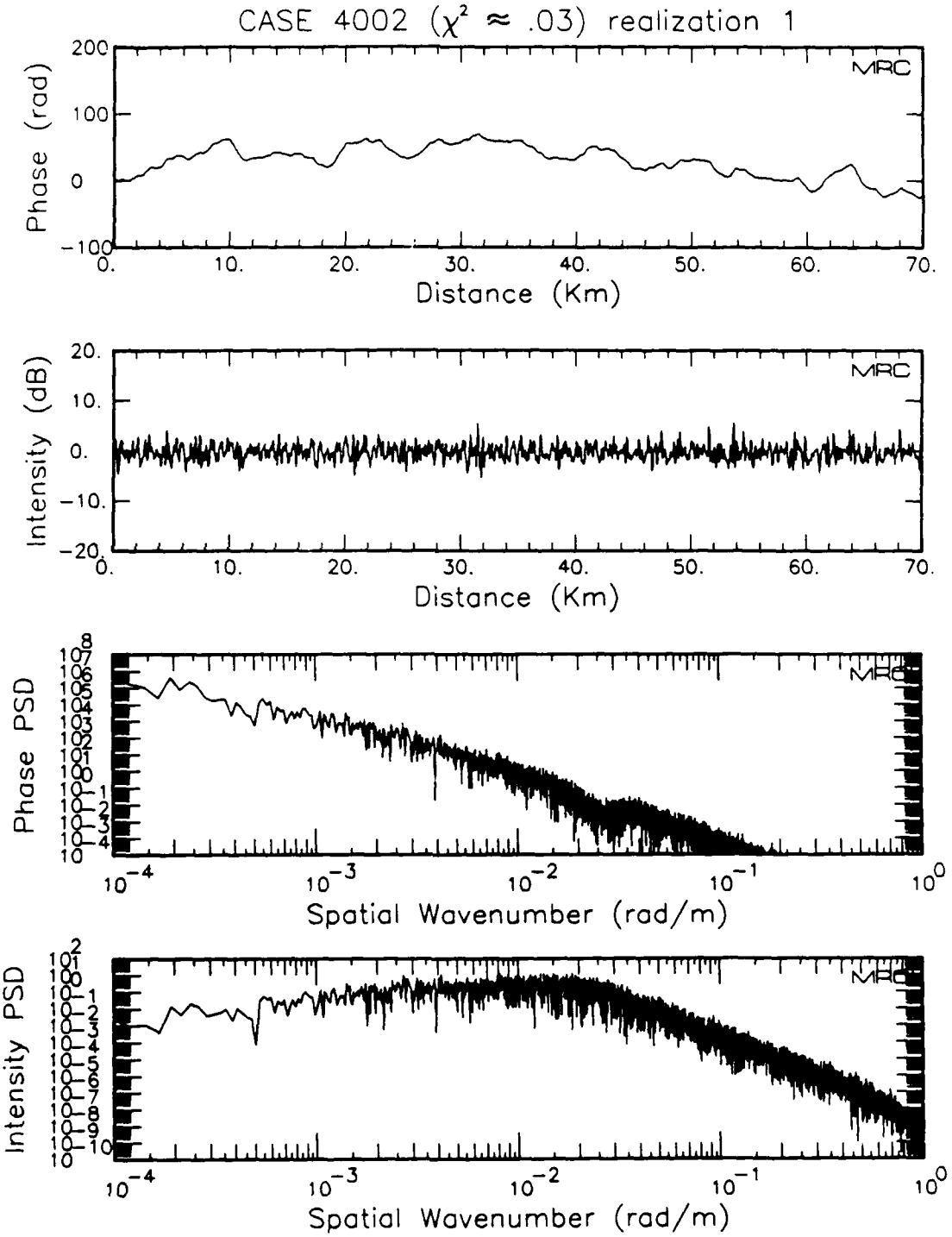

Figure 2. Plots of phase, intensity, and their respective power spectral densities for a realization with $\langle \chi^2 \rangle = .03$ (10 GHz).

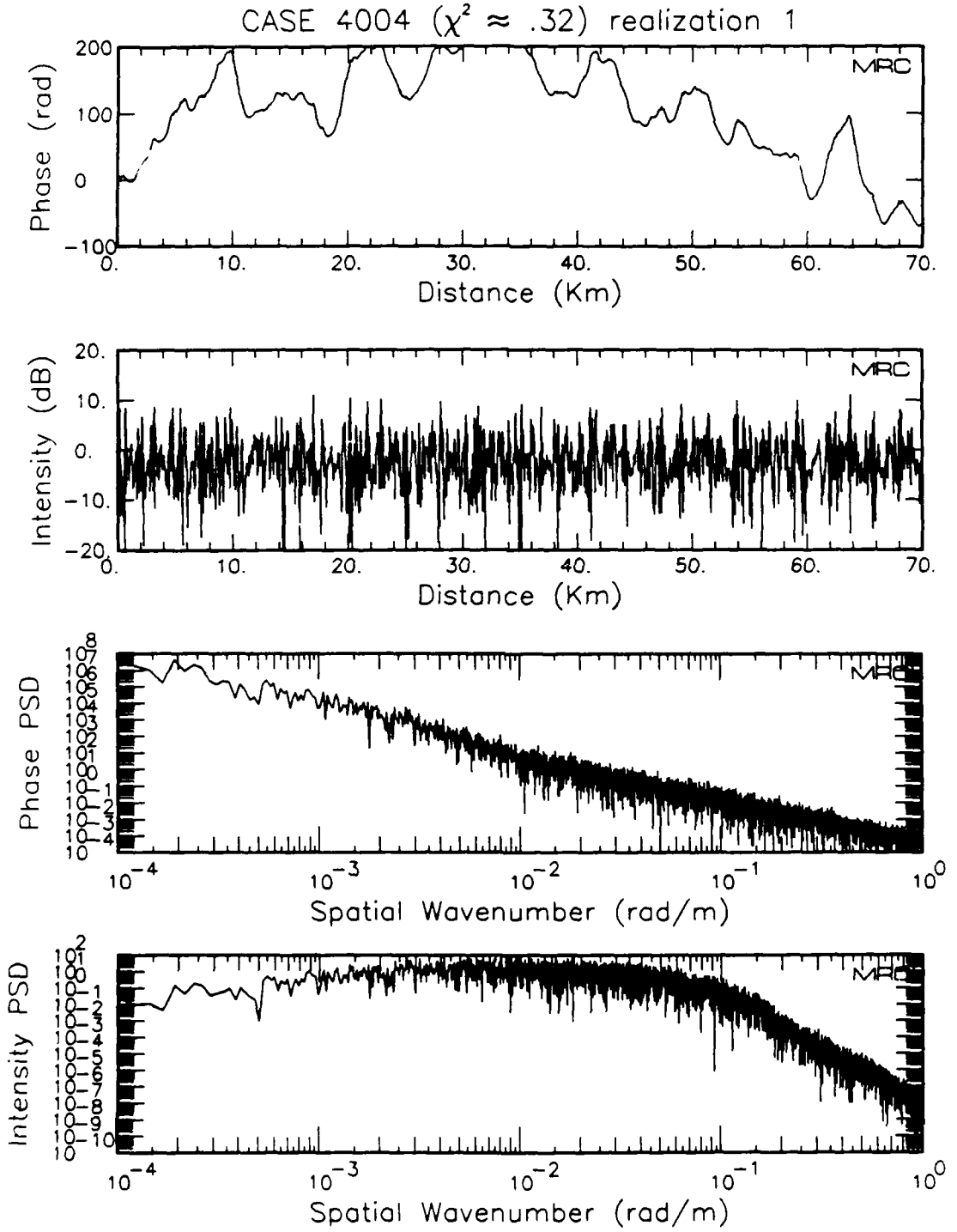

Figure 3. Plots of phase, intensity, and their respective power spectral densities for a realization with $\langle \chi^2 \rangle = .32$ (10 GHz).

and consist of small spikes with magnitude less than 5 dB. Signal phase as a function of distance is smooth compared to Figure 3, which is a more strongly scattered case.

In Figure 3, the phase fluctuations are much more extreme and there is a slow drift up from 0 to 30 km and then down again. This "TEC-wandering" or "phase-wandering" is due to large scale structure in the intervening layer.

The intensity plot of Figure 3 displays frequent 10 dB spikes and, more importantly, some instances of extremely sharp fades. For the strongest-scattering case simulated, these intensity fluctuations, due primarily to diffraction, begin to approach Rayleigh as can be seen by comparing the plots of Figure 4.

Figure 5 is a graph of average phase power spectral density at the receiver corresponding to the most weakly-scattered case at 10 GHz. It is apparent that the spectral density's slope is governed by $2n'$-1 for large spatial wavenumber and by $2n-1$ for smaller K, where n and n' are the respective intermediate and transition scale parameters that help define the index of refraction fluctuation power spectral density. The small "hump" at K = 3×10^{-2} is due to a purely geometrical Fresnel-filtering effect; it corresponds to the first Fresnel zone.

Evidence that the grid-spacing was chosen small enough to preserve phase information is given by the relatively small number of times that the phase changed by more than 90 degrees from grid-point to grid-point. For the worst case, the case of highest frequency and largest phase variance, there were only 242 of these "phase-slips" out of more than 138,000 points.

2.2 HOW TO ACCESS INFORMATION IN THE DATA BASE.

The MPS calculations produced 150 output files; that is, ten realizations for each of the fifteen cases of frequency and phase-variance. Analysis of these files revealed little variation between realizations within a given case. Therefore, considering the size of these files, and in keeping with previous procedures, only a subset of the total 150-file set was placed in the data base. The realizations chosen for inclusion were based on the calculated $\langle \chi^2 \rangle$ value for the case, where $\langle \chi^2 \rangle$ is the mean-square value of the logarithm of signal amplitude. Included for each case are the following files:

1. MPS⟨case_number⟩.AVG - the realization in which the measured $\langle \chi^2 \rangle$ fell closest to the average,

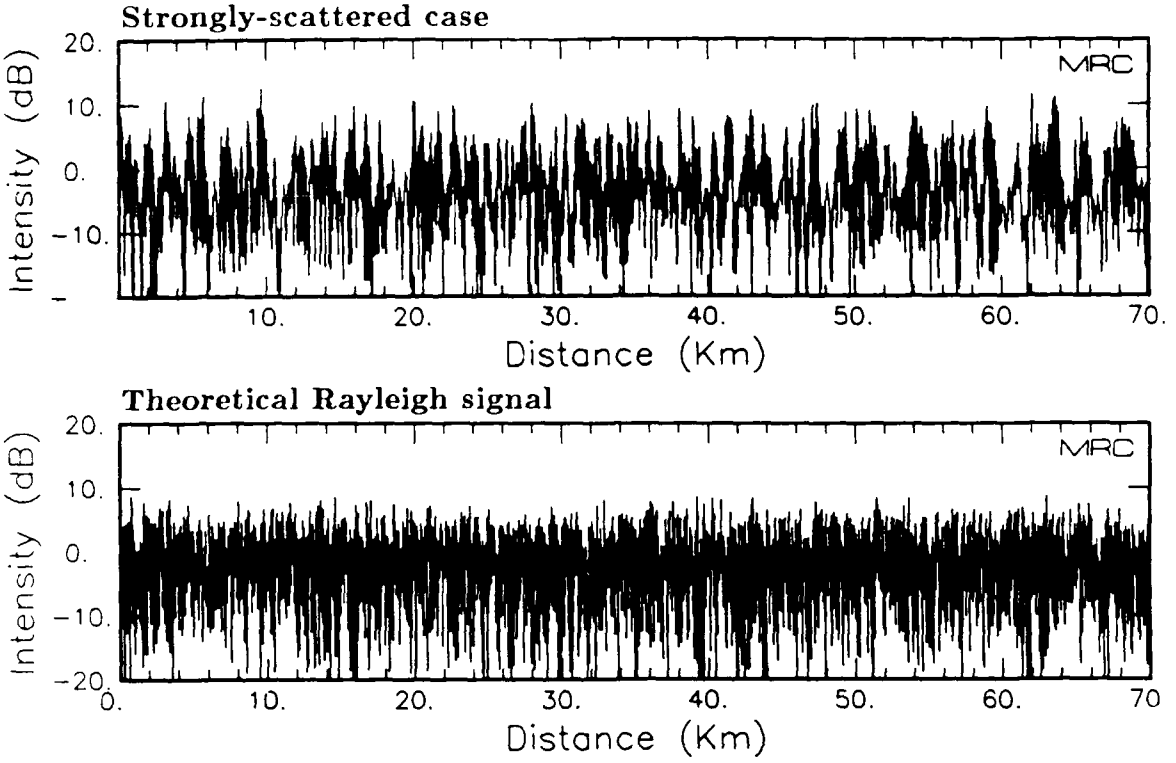

Figure 4. Strongly-scattered case compared to a theoretical Rayleigh signal.

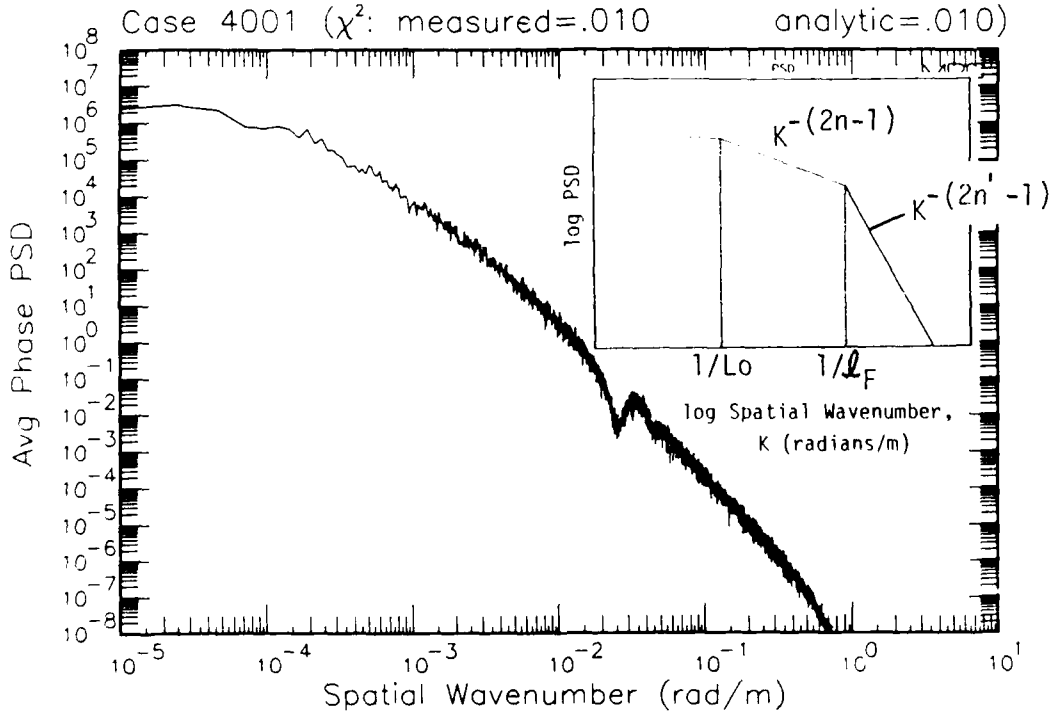

Figure 5. Theoretical slope structure in the phase PSD corresponding to the most weakly-scattered case (10 GHz).

2. MPS⟨case_number⟩.MAX – the realization with largest measured $\langle\chi^2\rangle$, and
3. MPS⟨case_number⟩.MIN – the realization with smallest measured $\langle\chi^2\rangle$.

Tables 2a-2c summarize the data generated. Each filename appears along with its layer's total phase variance and measured values of $\langle\chi^2\rangle$, S_4 index, and decorrelation distance.

The output files themselves each contain a simulation identification record, records containing problem definition data, and floating point realization data records, which are written as buffered blocks of (I,Q)-voltage level pairs. Appendix B provides details concerning the output file format and Appendix C lists a Fortran subroutine that may be used to read realization data into a simulation code.

Table 2a. Description and summary of 10 GHz data base.

Carrier Frequency = 10 GHz				
Filename	σ_ϕ^2 [rad^2]	$\langle\chi^2\rangle$	S_4	ℓ_0 [m]
average	6.20E+02	.00980	.201	191
mps4001.avg		.00987	.201	193
mps4001.max		.0104	.206	197
mps4001.min		.00940	.195	190
average	1.96E+03	.0312	.369	105
mps4002.avg		.0314	.370	106
mps4002.max		.0330	.378	107
mps4002.min		.0302	.355	104
average	6.20E+03	.103	.698	58.0
mps4003.avg		.104	.695	53.4
mps4003.max		.110	.722	59.4
mps4003.min		.0991	.675	57.9
average	1.96E+04	.315	1.12	32.4
mps4004.avg		.315	1.12	32.3
mps4004.max		.327	1.16	33.1
mps4004.min		.298	1.09	31.3
average	6.20E+04	.570	1.31	18.1
mps4005.avg		.569	1.29	18.9
mps4005.max		.578	1.34	16.7
mps4005.min		.558	1.27	17.6

Table 2b. Description and summary of 3.16 GHz data base.

Carrier Frequency = 3.16 GHz

Filename	σ_ϕ^2 [rad^2]	$\langle\chi^2\rangle$	S_4	ℓ_0 [m]
average	1.25E+02	.00983	.201	457
mps4006.avg		.00983	.200	495
mps4006.max		.0104	.206	411
mps4006.min		.00933	.195	453
average	3.95E+02	.0315	.366	243
mps4007.avg		.0316	.363	259
mps4007.max		.0333	.375	250
mps4007.min		.0299	.356	242
average	1.25E+03	.107	.678	132
mps4008.avg		.107	.664	140
mps4008.max		.115	.708	136
mps4008.min		.0989	.659	132
average	3.95E+03	.327	1.08	73.1
mps4009.avg		.327	1.03	77.3
mps4009.max		.346	1.11	73.6
mps4009.min		.313	1.07	71.3
average	1.25E+04	.559	1.24	40.7
mps4010.avg		.561	1.30	40.7
mps4010.max		.597	1.29	37.6
mps4010.min		.533	1.20	42.5

Table 2c. Description and summary of 1 GHz data base.

Carrier Frequency = 1 GHz

Filename	σ_ϕ^2 [rad^2]	$\langle\chi^2\rangle$	S_4	ℓ_0 [m]
average	2.73E+01	.00986	.200	1120
mps4011.avg		.00987	.199	1180
mps4011.max		.0108	.210	989
mps4011.min		.00902	.190	1210
average	8.64E+01	.0316	.361	563
mps4012.avg		.0317	.357	573
mps4012.max		.0351	.379	504
mps4012.min		.0290	.339	607
average	2.73E+02	.109	.648	296
mps4013.avg		.109	.655	301
mps4013.max		.121	.671	269
mps4013.min		.101	.598	317
average	8.64E+02	.331	1.01	160
mps4014.avg		.324	.990	156
mps4014.max		.372	1.06	147
mps4014.min		.306	.969	155
average	2.73E+03	.548	1.18	88.3
mps4015.avg		.545	1.18	85.4
mps4015.max		.605	1.27	81.2
mps4015.min		.515	1.13	86.4

SECTION 3

LIST OF REFERENCES

1. Dana, R.A., *ACIRF User's Guide, Volume 1: Theory and Examples*, DNA001-87-C-0169, MRC-R-1198, Mission Research Corporation, December 1988.

2. Dodson, R.E., D.J. Krueger, and F.W. Guigliano, *PRPSIM: A FORTRAN Code to Calculate Properties of Radio Wave Propagation in a Structured Ionized Medium, Volume II: Theory and Models*, MRC-R-1011, Mission Research Corporation, May 1987.

3. Knepp, D.L., *Propagation of Wide Bandwidth Signals Through Strongly Turbulent Ionized Media*, DNA-TR-81-78, MRC-R-671, Mission Research Corporation, March 1982.

4. Wittwer, L.A., *UHF Propagation Effects in Scintillation Environments*, AFWL-TR-76-304, Air Force Weapons Laboratory, August 1977.

5. Wittwer, L.A., *A Trans-Ionospheric Signal Specification for Satellite C^3 Applications, Volume III.*, DNA-IR-XX-XX, Defense Nuclear Agency, (in preparation).

APPENDIX A

THEORETICAL OVERVIEW

The scalar wave equation,

$$(\nabla^2 + k^2 n^2) E = 0$$

where

$$\nabla^2 = \frac{\partial^2}{\partial x^2} + \frac{\partial^2}{\partial z^2} \quad ,$$
$$k = \frac{2\pi}{\lambda} \quad ,$$

and $n = 1 + \Delta n$ is the index of refraction with Δn a small perturbation, describes a plane wave propagating in the z-direction through a medium assumed to consist of random striations that are infinitely extended in the y-direction (out of the page in Figure 6a).

This assumption, which effectively reduces the analysis to a two-dimensional geometry, is often a good one since the striated ionization tends to align itself with the earth's magnetic field and propagation before the Rayleigh limit is reached is primarily two-dimensional (the simulation can be easily extended to handle a three-dimensional geometry but would require considerably greater computational effort).

In Figure 6b, the ionized region has been partitioned into a number of thin layers, each perpendicular to the direction of propagation. Consider the ith layer, centered at $z = z_i$, with thickness Δz.

In order to analyze, first, the effect of the layer upon the wave's phase, the electric field is written in terms of complex amplitude and phase:

$$E(x, z, \omega) = U(x, z, \omega) e^{-ikz}$$

This has the effect of separating the free space propagation portion of the electric field from the phase-changing portion that is affected by the medium. Substituting into the scalar wave equation and making order of magnitude arguments leads to the parabolic wave equation:

$$\frac{\partial^2 U}{\partial x^2} - 2ik\frac{\partial U}{\partial z} + 2k^2 \Delta n(x, z, \omega) U = 0$$

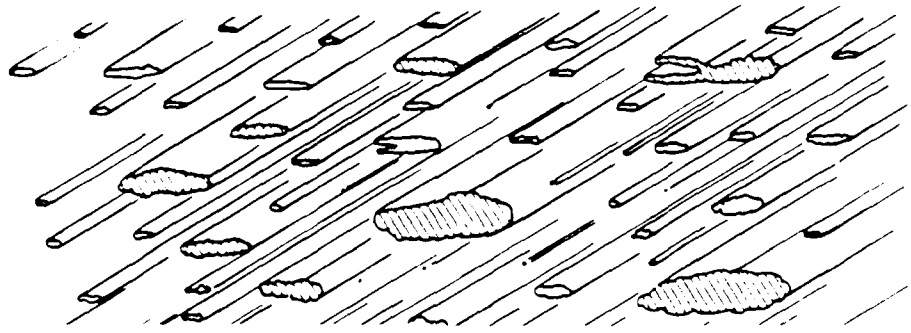

a.

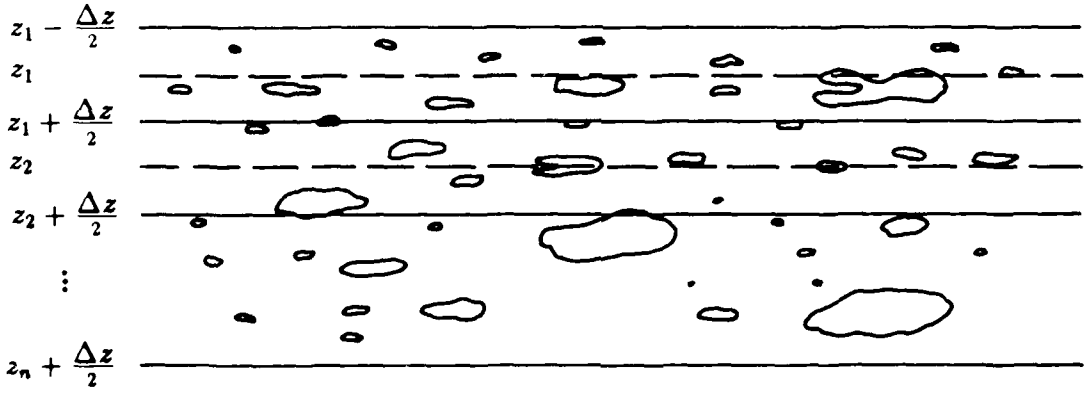

b.

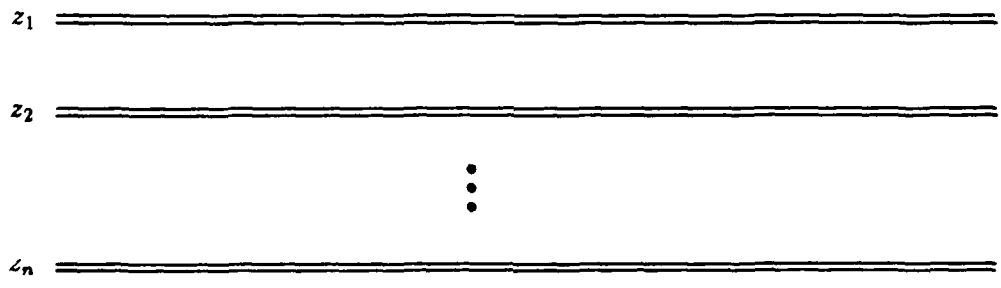

c.

Figure 6. Phase-screen representation of the ionized region.

Suppose the irregularities in each thin layer are now compressed into infinitesimally thin screens that preserve the phase-perturbing effect. The ionized medium is thus represented by a series of thin diffracting phase-screens separated by free space (Figure 6c).

For small Δz, the equation for propagation through the thin layer is obtained from the parabolic wave equation by neglecting the first term; that is, propagation effects within the thin layer have been ignored. The analysis focuses only on those terms governing the phase change induced by the medium's varying index of refraction. The resulting equation is easily solved by separation of variables:

$$U_+(x, z_i, \omega) = U_-(x, z_i, \omega) \exp\left\{-ik \int_{z_i - \frac{\Delta z}{2}}^{z_i + \frac{\Delta z}{2}} \Delta n(x, z', \omega) dz'\right\} \quad (1)$$

where U_- and U_+ denote the values of U as it enters and exits the phase-screen at z_i. Equation 1 states that the exiting wave's phase is a simple sum of phase change associated with the layer and the phase of the electric field at the entrance to the layer.

Turning now to the free-space propagation portion of the analysis, the last term of the parabolic wave equation can be ignored, and the resulting equation is easily solved by Fourier transform techniques:

$$\hat{U}_-(K, z_{i+1}, \omega) = \hat{U}_+(K, z_i, \omega) \exp\left[iK^2(z_{i+1} - z_i)/2k\right]$$

where the circumflex denotes the Fourier transform of U.

Taking the inverse transform leads to

$$U_-(x, z_{i+1}, \omega) = \int_{-\infty}^{\infty} \hat{U}_+(K, z_i, \omega) \exp\left[iK^2(z_{i+1} - z_i)/2k + iKx\right] dK$$

or in terms of the electric field

$$E_-(x, z_{i+1}, \omega) = e^{-iK(z_{i+1} - z_i)} \int_{-\omega}^{\omega} \hat{E}_+(K, z_i, \omega) \exp\left[iK^2(z_{i+1} - z_i)/2k + iKx\right] dK \quad (2)$$

Propagation of the electromagnetic wave from z_i to z_{i+1} has been decomposed into two parts: first, a pure phase change contribution, induced by irregularities in z_i's layer, calculated by adding the phase change indicated by Equation 1 to the phase of the electric field at the entrance to the phase-screen associated with z_i and second, a free-space propagation contribution given by Equation 2, which is carried out by Fourier transforming the phase-perturbed field, multiplying in K-space by

$e^{iK^2(z_{i+1}-z_i)/2k}$, and fast Fourier transforming. This two-step procedure is repeated at each screen, with the final free-space propagation terminating at the receiver plane.

Specific realizations of the random phase in Equation 1,

$$\phi(x) = -k \int_{z_i - \frac{\Delta z}{2}}^{z_i + \frac{\Delta z}{2}} \Delta n(x, z') dz'$$

that define a phase-screen are obtained by sampling a distribution of phase shifts whose statistical properties are specified by the power spectral density of the electron density irregularities. Specifically, the one-dimensional phase PSD is related to the three-dimensional in-situ electron density fluctuation PSD as follows:

First, the three-dimensional electron density fluctuation PSD is given by (see Reference 5 for complete definitions of terms)

$$PSD_{N_e}(K_x, K_y, K_z) = \frac{8\pi^{3/2} \left\langle \Delta N_e^2 \right\rangle N_3(n, n', R) L_r L_s L_t \Gamma(n)}{\Gamma(n - 3/2)} \quad /$$

$$\left[(1 + K_x^2 L_x^2 + K_y^2 L_y^2 + K_z^2 L_z^2 + 2L_{xy} K_x K_y + 2L_{xz} K_x K_z + 2L_{yz} K_y K_z)^n \right.$$

$$\left. (1 + K_x^2 \ell_x^2 + K_y^2 \ell_y^2 + K_z^2 \ell_z^2 + 2\ell_{xy} K_x K_y + 2\ell_{xz} K_x K_z + 2\ell_{yz} K_y K_z)^{n'-n} \right]$$

where normalization terms have been introduced to make

$$\int PSD_{N_e} \frac{d\vec{K}}{8\pi^3} = \overline{\Delta N_e^2}$$

By making use of the Markov approximation (i.e., by assuming that PSD_{N_e} is delta-correlated in the z-direction), the two-dimensional differential phase spectrum can be directly related to the three-dimensional electron density fluctuation PSD:

$$\frac{dP_\phi}{dz}(K_x, K_y) = r_e^2 \lambda^2 PSD_{N_e}(K_x, K_y, K_z = 0)$$

Finally, the one-dimensional phase PSD can be obtained by carrying out the integration over the spatial wavenumber K_y (again, Reference 5 contains complete definitions of terms):

$$\begin{aligned} \frac{dP_\phi(K_x)}{dz} &= \int_{-\infty}^{\infty} \frac{dP_\phi(K_x, K_y)}{dz} \frac{dK_y}{2\pi} \\ &= \frac{d\sigma_\phi^2}{dz} \frac{2\sqrt{\pi} N_2 \Gamma(n - 1/2)(1 + 6.4/n')L_{z'}}{\Gamma(n-1)(1 + 6.4/n)(1 + L^2 K_x^2)^{n-.5}(d^2 + \ell^2 K_x^2)^{n'-n}} \end{aligned}$$

A practical technique for generating the (discrete) Fourier transform of a given phase-screen realization makes use of the discrete spectral density of the desired phase:

$$\hat{\phi}(m\Delta k) = r_m \left[S(m\Delta k)L/2\pi\right]^{1/2}$$

where $r_m = \sqrt{1/2}(g_{1m} + ig_{2m})$, g_{1m} and g_{2m} are samples from a standard normal distribution, and $S(m\Delta k)$ is the discrete spectral density corresponding to a given layer; i.e.,

$$\Delta P_\phi = \frac{dP_\phi}{dz}\Delta z$$

and $S(m\Delta k)$ is the discrete version of ΔP_ϕ.

The "phase-variance-per-screen" quantity input to MPS is obtained by integrating differential phase variance, $\frac{d\sigma_\phi^2}{dz}$, over the thickness of the layer represented by the screen.

MPS can handle the regions in propagation space that include weak scattering to near Rayleigh scattering. Its use of FFTs make MPS relatively fast and inexpensive, so many cases can be run. Although MPS is practical only for two-dimensional problems due to computer considerations, this is not a serious problem for reasons mentioned earlier.

The most serious limitation on the MPS method derives from the practical limitation on the smallness of Δx, the transverse mesh-spacing. As the propagation environment degrades, the distance over which significant phase or amplitude fluctuations occur becomes smaller. In practice it is required that $\Delta x < \ell_0$. This restriction limits the severity of effects that can be accurately simulated by the MPS method.

Fortunately, calculations reveal that UHF signals become Rayleigh before Δx becomes so small as to make MPS calculations impractical. In the Rayleigh regime, other simulation methods, such as ACIRF (Reference 1), can be employed.

APPENDIX B

MPS OUTPUT FILE DESCRIPTION

This appendix describes the format of signal realization data base files. For a specific request, an ANSI standard tape will be written with data in ASCI format (or some other mutually agreeable format). This standard data format was chosen over a machine-specific format to alleviate the need for support of the wide range of computer systems in use by government contractors. In addition to the tape, a small Fortran program will be included to convert the specific format to the unformatted style used in this appendix. The overall file structure is as described below (note that each output file contains a single realization):

Record	
1	character identification record
2	floating point record A (problem definition data)
3	floating point record B (detailed problem definition data)
	———
4	record A (for check purposes)
5	floating point realization data record C1
	———
6	record A
7	record C2
	———
	...

	A	B	A	C1	A	C2	...	A	C_n
1	2	3	4	5	6	7		n+3	n+4

On the following pages a detailed description of each of the above records is provided. For each record, the Fortran write statements used to produce the record are shown and followed by a tabular description of the variables written.

```
------------------------------
character identification record
------------------------------


      CHARACTER  IDENT*80
      INTEGER    NID
C
C
      NID = 80
      WRITE (1) NID,IDENT(1:NID)
```

Variable	Description
NID	number of characters in IDENT string (nominally 80)
IDENT	alphanumeric identification of simulation

```
------------------------------------------------
floating point record A (problem definition data)
------------------------------------------------

      INTEGER     I,N1
      REAL        RDAT1
C
      DIMENSION   RDAT1(28)
C
C
      N1 = 28
      WRITE (1) N1,(RDAT1(I),I=1,N1)
```

	Variable	Description
	N1	number of floating point numbers in RDAT1 array (currently 28)
	RDAT1(1:N1)	floating point problem definition data
	where	
	RDAT1(1) = SOURCE	simulation source code identifier: 1. = MPS
	RDAT1(2) = CASEID	case identifier
	RDAT1(3) = FC	carrier frequency (Hz)
*	RDAT1(4) = 0.	
*	RDAT1(5) = 0.	
	RDAT1(6) = DLX	decorrelation distance in x-direction (m)
*	RDAT1(7) = 0.	
	RDAT1(8) = CHIBAR	$\langle \chi^2 \rangle$ - mean square log amplitude fluctuation of realization

	Variable	Description
	RDAT1(9) = S_4	scintillation index of realization
	RDAT1(10) = XLENG	grid length (m)
	RDAT1(11) = NGRIDX	number of grid points
	RDAT1(12) = DELTAX	grid point spacing (m)
*	RDAT1(13) = 0.	
*	RDAT1(14) = 0.	
*	RDAT1(15) = 0.	
	RDAT1(16) = RNRLX	number of grid points per DLX
	RDAT1(17) = NFREQ	number of frequencies
	RDAT1(18) = FREQ0	lowest frequency (Hz)
	RDAT1(19) = DELTAF	delta frequency (Hz)
*	RDAT1(20) = 0.	
*	RDAT1(21) = 0.	
*	RDAT1(22) = 0.	
	RDAT1(23) = RAN1	random number seed 1
	RDAT1(24) = RAN2	random number seed 2
	RDAT1(25) = MAXBUF	maximum buffer size (real words) [buffer size required to read largest realization record in this file]
*	RDAT1(26) = 0.	
*	RDAT1(27) = 0.	
	RDAT1(28) = VERS	code version number

* denotes quantities not calculated by the MPS code. Realization data generated by both the MPS and ACIRF computer codes share a common file format. When a particular parameter is not calculated by the source code the value is assigned zero.

```
------------------------------------------------------------
floating point record B (detailed problem definition data)
------------------------------------------------------------


      INTEGER     I,N2
      REAL        RDAT2
C
      DIMENSION   RDAT2(250)
C
C
      N2 = 250
      WRITE (1) N2,(RDAT2(I),I=1,N2)
```

Variable	Description
N2	number of floating point numbers in RDAT2 array (not to exceed 250)
RDAT2(1:N2)	floating point detailed problem definition data (Note that this data is primarily meant to aid in detailed problem description for internal MRC use and archive.)

where RDAT2(1:N2) are yet to be determined by the MPS and ACIRF code custodians.

```
------------------------------------------------------------
floating point realization data records (buffered due to size)
------------------------------------------------------------

      INTEGER     I,K,LFTOVR,MAXBUF,N1,NGRIDX
      REAL        RDAT1,REALI,REALQ
C
      PARAMETER   (NGRIDX = "number of grid points")
      PARAMETER   (MAXBUF = "data buffer size -- must be even")
C
      DIMENSION   RDAT1(28),REALI(NGRIDX),REALQ(NGRIDX)
C
C
      N1      = 28
      NUMBLK = NGRIDX*2/MAXBUF
C
      DO I = 1, NUMBLK
        WRITE (1) N1,(RDAT1(K),K=1,N1)
        WRITE (1) MAXBUF,
     &   (REALI((I-1)*MAXBUF+K),REALQ((I-1)*MAXBUF+K),K=1,MAXBUF/2)
      ENDDO
C
      LFTOVR = MOD (MAXBUF,NGRIDX*2)
      IF (LFTOVR.GT.0) THEN
        WRITE (1) N1,(RDAT1(K),K=1,N1)
        WRITE (1) LFTOVR,
     &   (REALI(NUMBLK*MAXBUF+K),REALQ(NUMBLK*MAXBUF+K),k=1,LFTOVR/2)
      ENDIF
```

Variable	*Description*
N1	number of floating point numbers in RDAT1 array (currently 28)
RDAT1(1:N1)	floating point problem definition data (each of these records is the same as the 2nd record in the file and is used as a means of verifying that the data file has been read in correctly)
NGRIDX	number of grid points
MAXBUF	buffer length of realization data record (words)
NUMBLK	number of realization data record blocks (those of length MAXBUF)
LFTOVR	number of left over realization data (only written when MAXBUF not a factor of NGRIDX)
	Note that the following data were written as I,Q pairs (I1,Q1, I2,Q2, I3,Q3, ...)
REALI()	array of floating point realization data (I voltage)
REALQ()	array of floating point realization data (Q voltage)

APPENDIX C

FORTRAN SUBROUTINE FOR SAMPLING REALIZATIONS

This appendix lists a sample Fortran subroutine for use in reading MPS or ACIRF realization data into a simulation code. The prospective user may find the following advisory comments useful.

If Δx is the reciever plane mesh spacing, then there are $\frac{\ell_0}{\Delta x}$ mesh points per decorrelation distance (note that ℓ_0 and Δx are located in positions 6 and 12 respectively of the array RDAT1; see the description of floating point record A in the previous appendix). For a given decorrelation time τ_0, the mesh point index corresponding to a particular time t of interest is given by $ITIME = \left(\frac{t}{\tau_0}\right)\left(\frac{\ell_0}{\Delta x}\right)$. The subroutine interpolates I,Q data from values at bracketing mesh points.

If the sample desired falls beyond the extent of the realization data, then the subroutine wraps the realization around to simulate a longer run.

If one prefers to access the realization data in the spatial domain rather than in the time domain, one can simply call SAMPLE with the time arguement set appropriately; i.e., $t = \left(\frac{\tau_0}{\ell_0}\right)(k\Delta x)$. Here, the quantity $(k\Delta x)$ is distance in the receiver plane, and k is the mesh point index.

```
      SUBROUTINE SAMPLE (IUNIT,FILEIN,RESET,TAUO,TIME,VI,VQ)
*
**********************************************************************
*                                                                    *
*     Fortran subroutine to get I and Q voltages from MPS or ACIRF   *
*     data files.                                                    *
*                                                                    *
*       INPUTS from argument list:                                   *
*     IUNIT  = logical unit number for input file                    *
*     FILEIN = input file name                                       *
*     RESET  = logical reset flag (should be set to TRUE by calling  *
*              routine when a new file is specified or a new run is  *
*              to be started; will be set to FALSE by this routine.) *
*     TAUO   = scintillation decorrelation time (s)                  *
```

```
*     TIME   = time of I-Q data relative to beginning of file (s)      *
*                                                                      *
*       OUTPUTS to argument list:                                      *
*     VI,VQ  = inphase and quadrature voltage samples                  *
*                                                                      *
************************************************************************
*
      CHARACTER FILEIN*(*),IDENT*80
*
      LOGICAL RESET
*
      DATA NIQ/0/
*     maximum buffer size
      PARAMETER (IBUF = 4096)
*
      DIMENSION RDAT1(28),RDAT2(250),REALI(0:IBUF/2),REALQ(0:IBUF/2),
     &          CKDAT(28)
*
      SAVE      RDAT2,REALI,REALQ,DELTAT,IMIN,IMAX,N1,NGRIDX,NTOTAL
*
************************************************************************
*
*     check reset flag (new file or new case)
    1 IF (RESET) THEN
          CLOSE (UNIT=IUNIT)
          OPEN  (UNIT=IUNIT,FILE=FILEIN,STATUS='OLD',FORM='UNFORMATTED')
*         read ID record
          READ (IUNIT) NID,IDENT(1:MINO(NID,80))
*         read record A
          READ (IUNIT) N1,(RDAT1(I),I=1,MINO(N1,28))
*         read record B
          READ (IUNIT) N2,(RDAT2(I),I=1,MINO(N2,250))
          IF (NID.GT.80) WRITE (*,*) 'ID record exceeds 80 characters'
          IF (N1.GT.28)  WRITE (*,*) 'Record A exceeds 28 words'
          IF (N2.GT.250) WRITE (*,*) 'Record B exceeds 250 words'
          IF (NID.GT.80 .OR. N1.GT.28 .OR. N2.GT.250) STOP
          MAXBUF = INT(RDAT1(25))
          IF (MAXBUF.GT.IBUF) THEN
              WRITE (*,*) 'Buffer size must be increased in SAMPLE'
              WRITE (*,*) 'Set IBUF = ',MAXBUF,' and recompile'
```

```
            STOP
          END IF
          ELZERO = RDAT1( 6)
          NGRIDX = RDAT1(11)
          NTOTAL = NGRIDX
          DELTAX = RDAT1(12)
          DELTAT = TAUO*DELTAX/ELZERO
          IMIN   = 0
          IMAX   = 0
          IF (NIQ.EQ.0) NIQ = IBUF/2
          RESET  = .FALSE.
        END IF
        ITIME = INT(TIME/DELTAT) + 1
*
         IF (ITIME.LT.1) THEN
          WRITE (*,*) 'Negative time cannot be used in SAMPLE'
          STOP
        END IF
*
        IF (ITIME.LT.IMIN) THEN
          WRITE (*,*) 'Warning: Time out of sequence in SAMPLE'
          WRITE (*,*) 'Will assume that you want to start over'
          RESET = .TRUE.
          GO TO 1
        END IF
*
*************************************************************************
*
*       Data is in buffer
      2 IF (ITIME.LT.IMAX) GO TO 4
        IF (ITIME.GE.NTOTAL) GO TO 3
*
*       read check record
        READ (IUNIT,END=99) NCK,(CKDAT(I),I=1,NCK)
        IF (NCK.NE.N1) THEN
          WRITE (*,*) 'Incorrect number of check words'
          STOP
        END IF
        DO I = 1, NCK
          IF (CKDAT(I).NE.RDAT1(I)) THEN
```

```
            WRITE (*,*) 'Check word error'
            STOP
         END IF
      END DO
*
*     Read I,Q data into buffer
      REALI(0) = REALI(NIQ)
      REALQ(0) = REALQ(NIQ)
      READ (IUNIT,END=99) NN,(REALI(I),REALQ(I),I=1,NN/2)
      NIQ = NN/2
      IMIN   = IMAX
      IMAX   = IMAX + NIQ
      GO TO 2
*
*     Wrap realization around for longer run
    3 REWIND (IUNIT)
      NTOTAL = NTOTAL + NGRIDX
      READ (IUNIT)
      READ (IUNIT)
      READ (IUNIT)
      GO TO 2
*
*************************************************************************
*
*     Interpolate I,Q data to specified time
    4 DT = AMOD(TIME,DELTAT) / DELTAT
      I  = ITIME - IMIN
      VI = REALI(I)*(1.-DT) + REALI(I+1)*(DT)
      VQ = REALQ(I)*(1.-DT) + REALQ(I+1)*(DT)
      RETURN
 99   STOP '** ERROR: END-OF-FILE ON READ IN SUBROUTINE SAMPLE **'
      END
```

APPENDIX D

DISCUSSION AND DETAILED SUMMARY OF THE MPS RUNS

This appendix summarizes the results of the MPS calculations in several ways.

First, **Tables 3a, 3b,** and **3c** (corresponding to realizations obtained at 10, 3.16, and 1 GHz, respectively) give the measured $\langle \chi^2 \rangle$ and ℓ_0 for all realizations and their theoretical values. The "theoretical" values referred to were calculated using methods implemented in PRPSIM (see Reference 2). The set of analysis points along a given line of sight were defined by the line of sight's intersection with the MPS thin layers. Theoretical values for $\langle \chi^2 \rangle$ were derived using the weak scintillation calculations implemented in PRPSIM, while the theoretical ℓ_0 was found by searching for the $\frac{1}{e}$ point of the autocorrelation function at the receiver.

The tables are followed by graphs (**figure 7**) of the results versus σ_ϕ^2 for the three frequencies. The average value for a set of realizations obtained for a single frequency and phase variance is indicated by the centered "X" and the individual realizations are indicated by the small dots. It can be seen that the agreement between the theoretical and measured values of ℓ_0 is excellent. For $\langle \chi^2 \rangle$ the agreement is excellent for values less than about .3. Since the theoretical formula has been derived assuming weak scintillation, the deviation for large $\langle \chi^2 \rangle$ is understandable.

Next, **figures 8-12** represent realizations obtained for a frequency of 10 GHz and are ordered, as are the other sets of figures that follow, from weakest to strongest scintillation (smallest to largest phase variance). The figures indicate the level of amplitude and phase variation across the receiver; they contain plots of signal phase and intensity, and their respective power spectral densities, for the realizations whose measured $\langle \chi^2 \rangle$ fell closest to the case average. These realizations correspond to the realizations on the tape labeled by MPS⟨case_number⟩.AVG. In a similar fashion, **figures 13-17** represent realizations obtained at 3.16 GHz, and **figures 18-22** represent the 1 GHz case.

For realizations with small $\langle\chi^2\rangle$ (.01 and .03) the fading and flaring intensity is generally confined to within 5 dB of the mean intensity. For stronger scintillation ($\langle\chi^2\rangle > .10$) the intensity is more severe;[1] as the scintillation begins to saturate ($\langle\chi^2\rangle \approx .5$) worst case fading and flaring is obtained. As the scintillation increases not only does the range of fading and flaring increase but the separation of the sharp fades or flares decreases. For the weak scintillation cases the phase PSD plot shows a slight kink near 10^{-2} rad/m. This kink represents the effect of Fresnel filtering at the first Fresnel zone.

Finally, **figures 23-27** provide a statistical comparison of the received power obtained from the MPS realizations with three theoretical distributions: (1) Rayleigh; (2) Rician; and (3) Nakagami-m. These comparisons make use of the MPS realizations from cases 4001-4005 (figures 8-12), whose carrier frequency is 10 GHz. The first plot in each figure compares the probability density functions (PDF) for the power fades and flares, and the second plot compares the cumulative distribution functions (CDF).

A histogram was accumulated for each of the ten realizations of a given case. In the figures, dots indicate the average bin values over the ten realizations, while bars show the standard deviation of bin-values. It can be seen from the figures that both Rician and Nakagami-m distributions provide somewhat better fits for $S_4 < 1.0$ than the Rayleigh distribution, with the Nakagami-m distribution offering a slightly more accurate model for the probability of fades.

For cases with $S_4 > 1.0$, the Rician model provides a better estimate for the probability of fades than the Nakagami-m, while the Nakagami-m closely matches the distribution of flares. The PDF shown in the last figure, CASE 4005, reflects the difference between the two intensity plots shown in figure 4 (page 10), where the theoretical Rayleigh signal lacks the flares of intensity greater than 10 dB that the strongly-scattered case possesses. The PDF shows a corresponding difference between the distribution of power greater than 5 dB for the MPS realizations (dots) and the Rayleigh distribution (solid line).

[1]Current DNA convention regards signals possessing $\langle\chi^2\rangle$ values greater than 0.1 as being "Rayleigh" signals. Rayleigh signals are generated by propagation paths penetrating significant nuclear effects regions. Typically a slight perturbation (towards increasing effects) in link/effects region geometry for weak, near-Rayleigh signals gives rise to rapidly increasing values for $\langle\chi^2\rangle$. The rapid change in $\langle\chi^2\rangle$ implies a corresponding rapid transition to Rayleigh statistics. Thus the 0.1 value is a conservative yet practical threshold.

The Rayleigh PDF and CDF are given by the formulas:

$$f(P) = \exp(-P) \quad , \quad F(P) = 1 - \exp(-P) \quad .$$

The Rayleigh functions are indicated on the plots by the short dashed lines.

The Rician PDF and CDF are given by the formulas:

$$\begin{aligned} f(P) &= \frac{1}{2\sigma^2} \exp\left\{-\frac{P+P_0}{2\sigma^2}\right\} I_0\left(\frac{\sqrt{PP_0}}{\sigma^2}\right) \\ F(P) &= \int_0^P f(P')\,dP' \\ &= 1 - Q\left(\frac{\sqrt{P_0}}{\sigma}, \frac{\sqrt{P}}{\sigma}\right) \\ Q(a,b) &\equiv \exp\left\{-\frac{a^2+b^2}{2}\right\} \sum_{k=0}^{\infty} \left(\frac{a}{b}\right)^k I_k(ab) \end{aligned}$$

The appropriate values P_0 and σ are obtained by deriving them from the measured scintillation index

$$S_4^2 = \frac{\langle P^2 \rangle - \langle P \rangle^2}{\langle P \rangle^2}$$

The formulas used are the following:

$$\begin{aligned} P_0 &= \sqrt{1 - S_4^2} \\ 2\sigma^2 &= 1 - \sqrt{1 - S_4^2} \end{aligned}$$

The Rician functions are indicated on the plots by the solid lines.

The Nakagami-m PDF and CDF are given by the formulas:

$$\begin{aligned} f(P) &= \frac{m^m P^{m-1}}{\Gamma(m)\langle P \rangle^m} \exp\left\{-\frac{mP}{\langle P \rangle}\right\} \\ F(P) &= \frac{\gamma\left(m, \frac{mP}{\langle P \rangle}\right)}{\Gamma(m)} \end{aligned}$$

where γ is the incomplete Gamma function and m is chosen by comparing the theoretical and measured values of the scintillation index:

$$m = \frac{1}{S_4^2}$$

The Nakagmai-m functions are indicated on the plots by the long dashed lines.

Table 3a. Detailed MPS realization summary of cases 4001-4005 (10 GHz).

Case	Total Phase Variance [rad^2]	Realization	$\langle\chi^2\rangle$	S_4	ℓ_0 [m]
4001	6.20E+02	1	.00990	.201	194
		2	.00965	.200	196
		3	.00993	.203	174
		4	.00987 (AVG)	.201	193
		5	.00970	.203	183
		6	.00960	.198	203
		7	.00940 (MIN)	.195	190
		8	.00989	.202	185
		9	.0104 (MAX)	.206	197
		10	.00966	.199	199
		Average	.00980	.201	191
		Theory	.00959		196
4002	1.96E+03	1	.0315	.367	106
		2	.0307	.368	107
		3	.0315	.376	96.0
		4	.0314 (AVG)	.370	106
		5	.0308	.376	101
		6	.0305	.364	111
		7	.0302 (MIN)	.355	104
		8	.0316	.372	102
		9	.0330 (MAX)	.378	107
		10	.0308	.365	109
		Average	.0312	.369	105
		Theory	.0303		108
4003	6.20E+03	1	.104	.689	58.6
		2	.101	.700	59.2
		3	.104 (AVG)	.695	53.4
		4	.105	.707	58.5
		5	.102	.707	56.1
		6	.100	.687	61.2
		7	.0991 (MIN)	.674	57.9
		8	.105	.704	56.6
		9	.110 (MAX)	.722	59.4
		10	.101	.689	60.4
		Average	.103	.698	58.0
		Theory	.0959		59.7

Table 3a. Detailed MPS realization summary of cases 4001-4005 (10 GHz) (continued).

Case	Total Phase Variance [rad^2]	Realization	$\langle\chi^2\rangle$	S_4	ℓ_0 [m]
4004	1.96E+04	1	.319	1.15	32.7
		2	.320	1.11	33.0
		3	.317	1.14	29.8
		4	.322	1.11	32.6
		5	.298 (MIN)	1.09	31.3
		6	.306	1.12	34.1
		7	.315 (AVG)	1.12	32.3
		8	.313	1.10	31.6
		9	.327 (MAX)	1.16	33.1
		10	.309	1.11	33.7
		Average	.315	1.12	32.4
		Theory	.303		33.4
4005	6.20E+04	1	.574	1.37	18.3
		2	.563	1.28	18.4
		3	.578 (MAX)	1.34	16.7
		4	.572	1.32	18.3
		5	.558 (MIN)	1.27	17.6
		6	.573	1.27	19.1
		7	.571	1.33	18.1
		8	.570	1.31	17.8
		9	.568	1.29	18.5
		10	.569 (AVG)	1.29	18.9
		Average	.570	1.31	18.1
		Theory	.959		18.7

Table 3b. Detailed MPS realization summary of cases 4006-4010 (3.16 GHz).

Case	Total Phase Variance [rad^2]	Realization	$\langle\chi^2\rangle$	S_4	ℓ_0 [m]
4006	1.25E+02	1	.00990	.200	469
		2	.00969	.200	468
		3	.0104 (MAX)	.206	411
		4	.00978	.200	463
		5	.00972	.202	436
		6	.00983 (AVG)	.200	495
		7	.00933 (MIN)	.195	453
		8	.00987	.201	440
		9	.0103	.205	473
		10	.00950	.197	478
		Average	.00983	.201	457
		Theory	.0960		471
4007	3.95E+02	1	.0318	.364	246
		2	.0311	.364	249
		3	.0332	.376	221
		4	.0314	.366	245
		5	.0309	.372	232
		6	.0316 (AVG)	.363	259
		7	.0299 (MIN)	.356	242
		8	.0317	.368	235
		9	.0333 (MAX)	.375	250
		10	.0304	.357	253
		Average	.0315	.366	243
		Theory	.0304		249
4008	1.25E+03	1	.109	.671	134
		2	.103	.674	135
		3	.112	.695	121
		4	.108	.680	133
		5	.103	.680	128
		6	.107 (AVG)	.664	140
		7	.0989 (MIN)	.659	132
		8	.108	.692	129
		9	.115 (MAX)	.708	136
		10	.104	.659	138
		Average	.107	.678	132
		Theory	.0960		136

Table 3b. Detailed MPS realization summary of cases 4006-4010 (3.16 GHz) (continued).

Case	Total Phase Variance [rad^2]	Realization	$\langle\chi^2\rangle$	S_4	ℓ_0 [m]
4009	3.95E+03	1	.346 (MAX)	1.11	73.6
		2	.315	1.05	74.5
		3	.344	1.10	67.1
		4	.331	1.10	73.5
		5	.313	1.04	70.6
		6	.327 (AVG)	1.03	77.3
		7	.314	1.08	72.9
		8	.313 (MIN)	1.07	71.3
		9	.343	1.09	74.7
		10	.320	1.08	76.1
		Average	.327	1.08	73.1
		Theory	.304		75.1
4010	1.25E+04	1	.571	1.28	41.0
		2	.540	1.21	41.4
		3	.597 (MAX)	1.29	37.6
		4	.569	1.24	40.9
		5	.551	1.23	39.4
		6	.557	1.23	43.0
		7	.561 (AVG)	1.30	40.7
		8	.553	1.24	39.9
		9	.563	1.20	41.5
		10	.533 (MIN)	1.20	42.5
		Average	.559	1.24	40.7
		Theory	.960		41.9

Table 3c. Detailed MPS realization summary of cases 4011-4015 (1 GHz).

Case	Total Phase Variance [rad^2]	Realization	$\langle\chi^2\rangle$	S_4	ℓ_0 [m]
4011	2.73E+01	1	.00987(AVG)	.199	1180
		2	.00990	.198	1140
		3	.0108 (MAX)	.210	989
		4	.00981	.201	1170
		5	.0101	.205	1050
		6	.00902 (MIN)	.190	1210
		7	.00974	.199	1130
		8	.00948	.197	1060
		9	.0102	.204	1200
		10	.00969	.198	1170
		Average	.00986	.200	1120
		Theory	.00957		1190
4012	8.64E+01	1	.0317	.358	581
		2	.0317 (AVG)	.357	573
		3	.0351 (MAX)	.379	504
		4	.0315	.363	567
		5	.0323	.369	534
		6	.0290 (MIN)	.339	607
		7	.0313	.357	560
		8	.0303	.359	540
		9	.0325	.369	594
		10	.0312	.356	589
		Average	.0316	.361	563
		Theory	.0302		582
4013	2.73E+02	1	.109 (AVG)	.655	301
		2	.107	.637	304
		3	.121 (MAX)	.671	269
		4	.110	.657	298
		5	.110	.649	282
		6	.101 (MIN)	.598	317
		7	.107	.640	295
		8	.104	.660	286
		9	.111	.667	307
		10	.106	.642	309
		Average	.109	.648	296
		Theory	.0957		304

Table 3c. Detailed MPS realization summary of cases 4011-4015 (1 GHz) (continued).

Case	Total Phase Variance [rad^2]	Realization	$\langle\chi^2\rangle$	S_4	ℓ_0 [m]
4014	8.64E+02	1	.351	1.05	162
		2	.317	.996	164
		3	.372 (MAX)	1.06	147
		4	.323	1.02	161
		5	.306 (MIN)	.969	155
		6	.314	.944	170
		7	.340	1.01	160
		8	.324 (AVG)	.990	156
		9	.321	1.02	165
		10	.341	1.02	168
		Average	.331	1.01	160
		Theory	.302		165
4015	2.73E+03	1	.554	1.20	88.7
		2	.516	1.14	89.5
		3	.605 (MAX)	1.27	81.2
		4	.538	1.15	88.5
		5	.545 (AVG)	1.18	85.4
		6	.580	1.17	93.7
		7	.565	1.27	88.2
		8	.515 (MIN)	1.13	86.4
		9	.534	1.12	90.0
		10	.522	1.17	92.4
		Average	.548	1.18	88.3
		Theory	.957		90.7

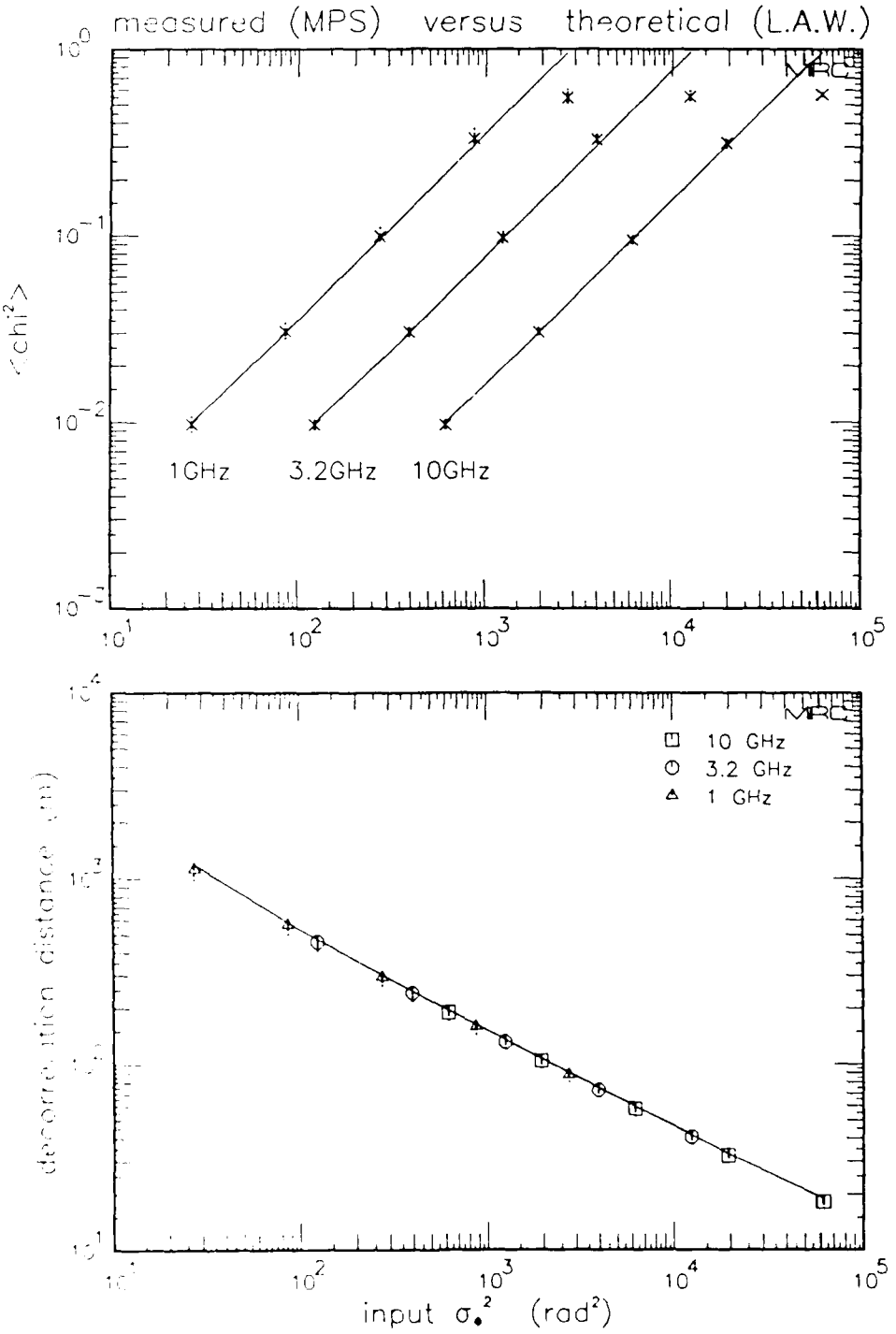

Figure 7. Comparison of theoretical and measured values for $\langle \chi^2 \rangle$ and ℓ_0.

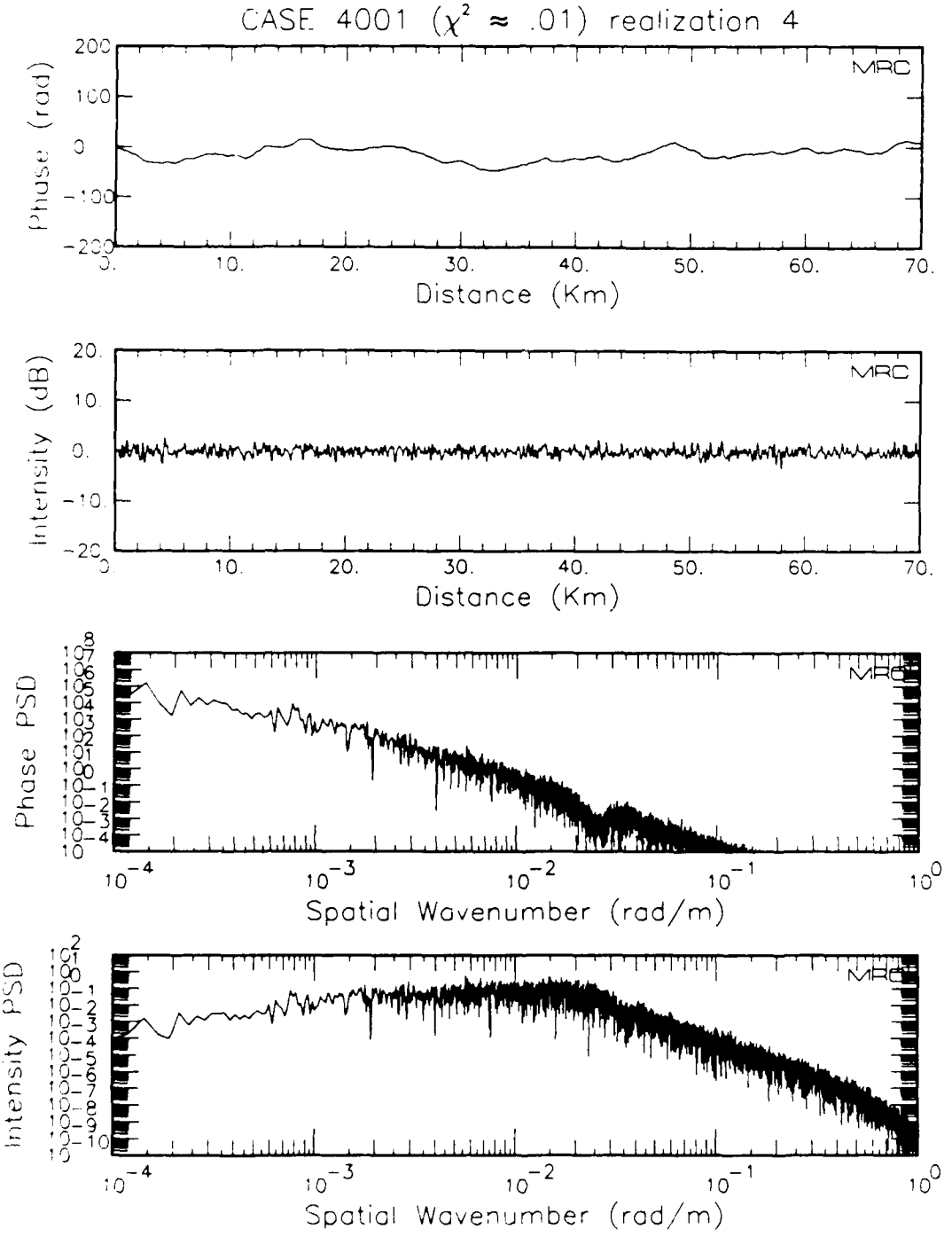

Figure 8. Representative phase, intensity, and power spectral density plots for case 4001.

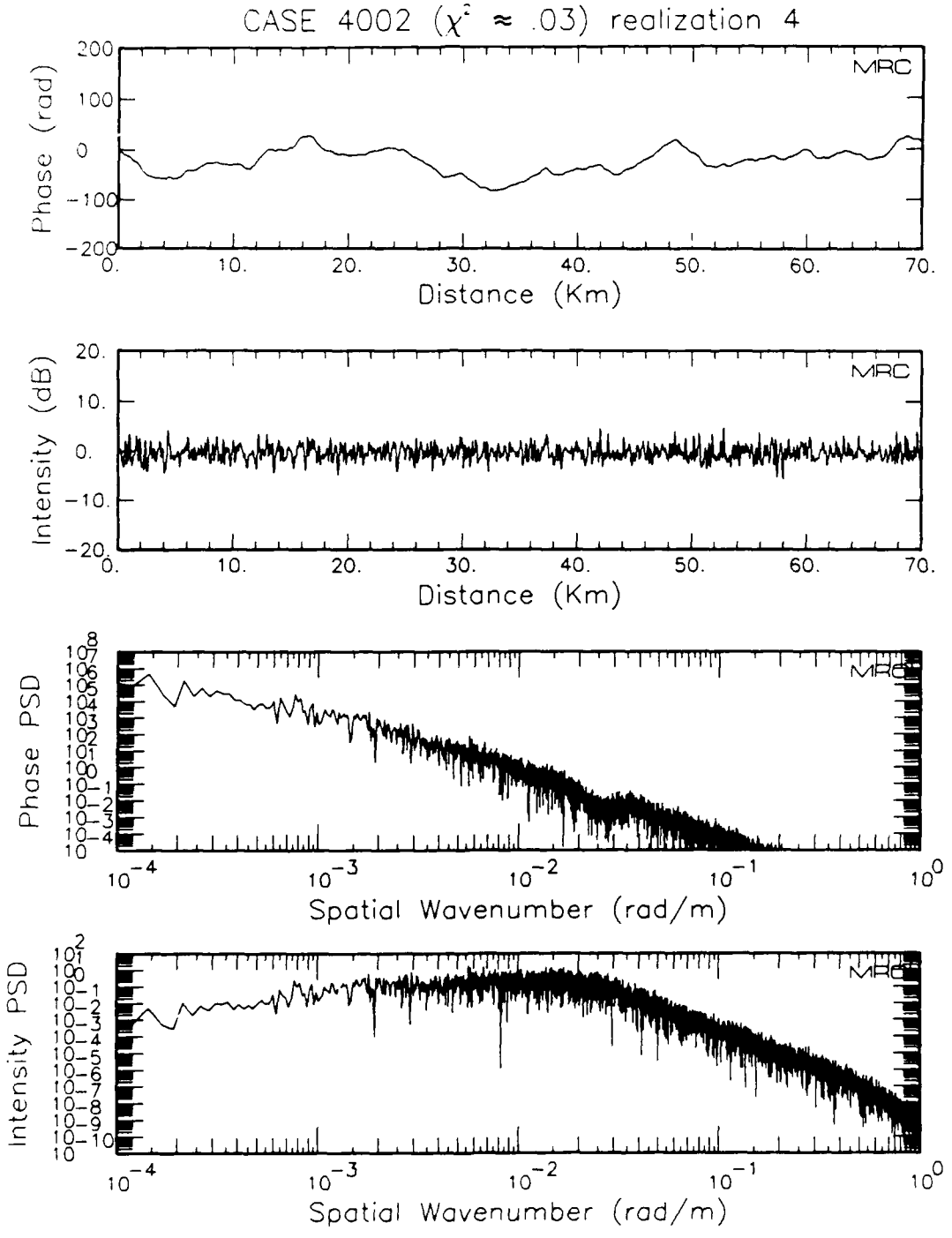

Figure 9. Representative phase, intensity, and power spectral density plots for case 4002.

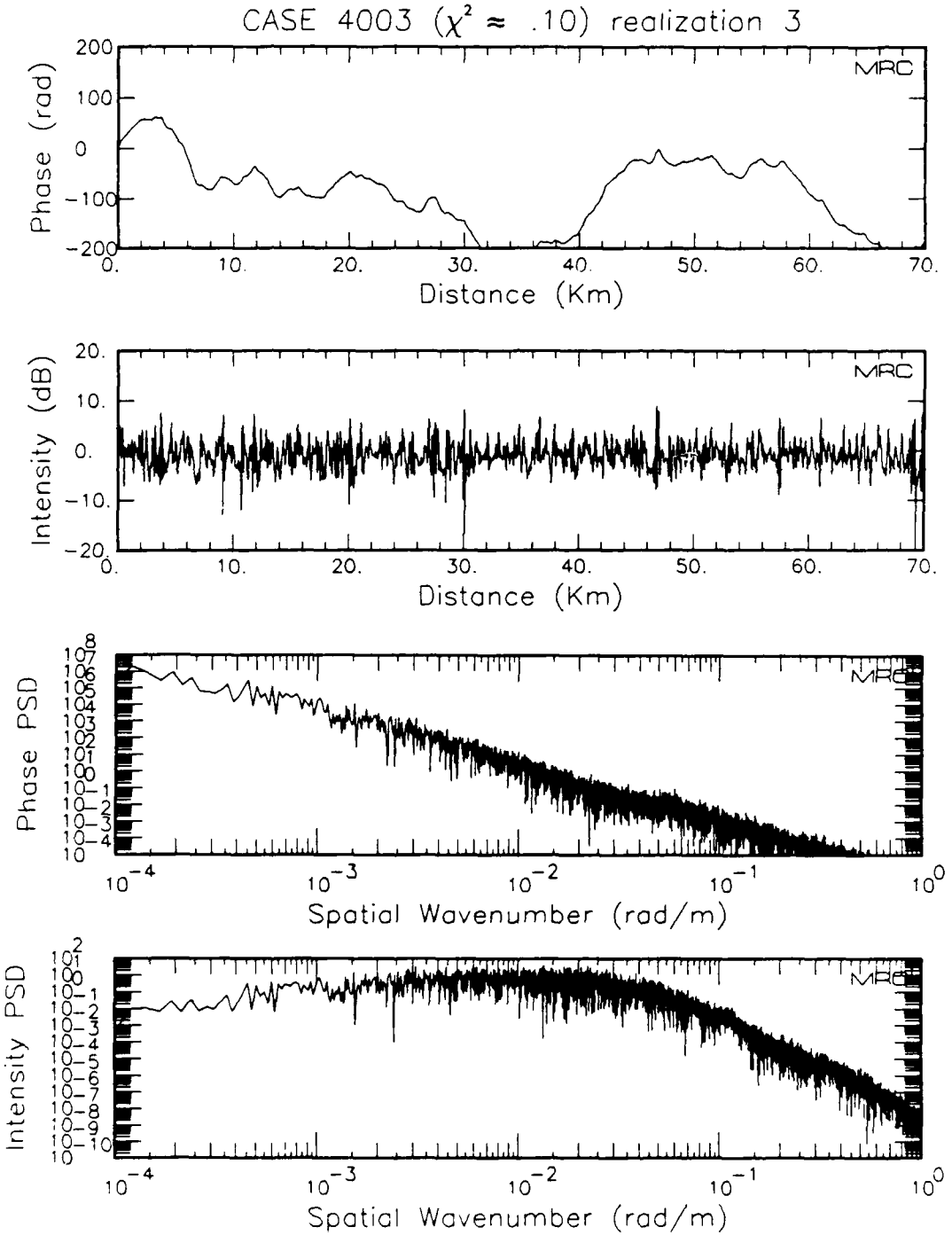

Figure 10. Representative phase, intensity, and power spectral density plots for case 4003.

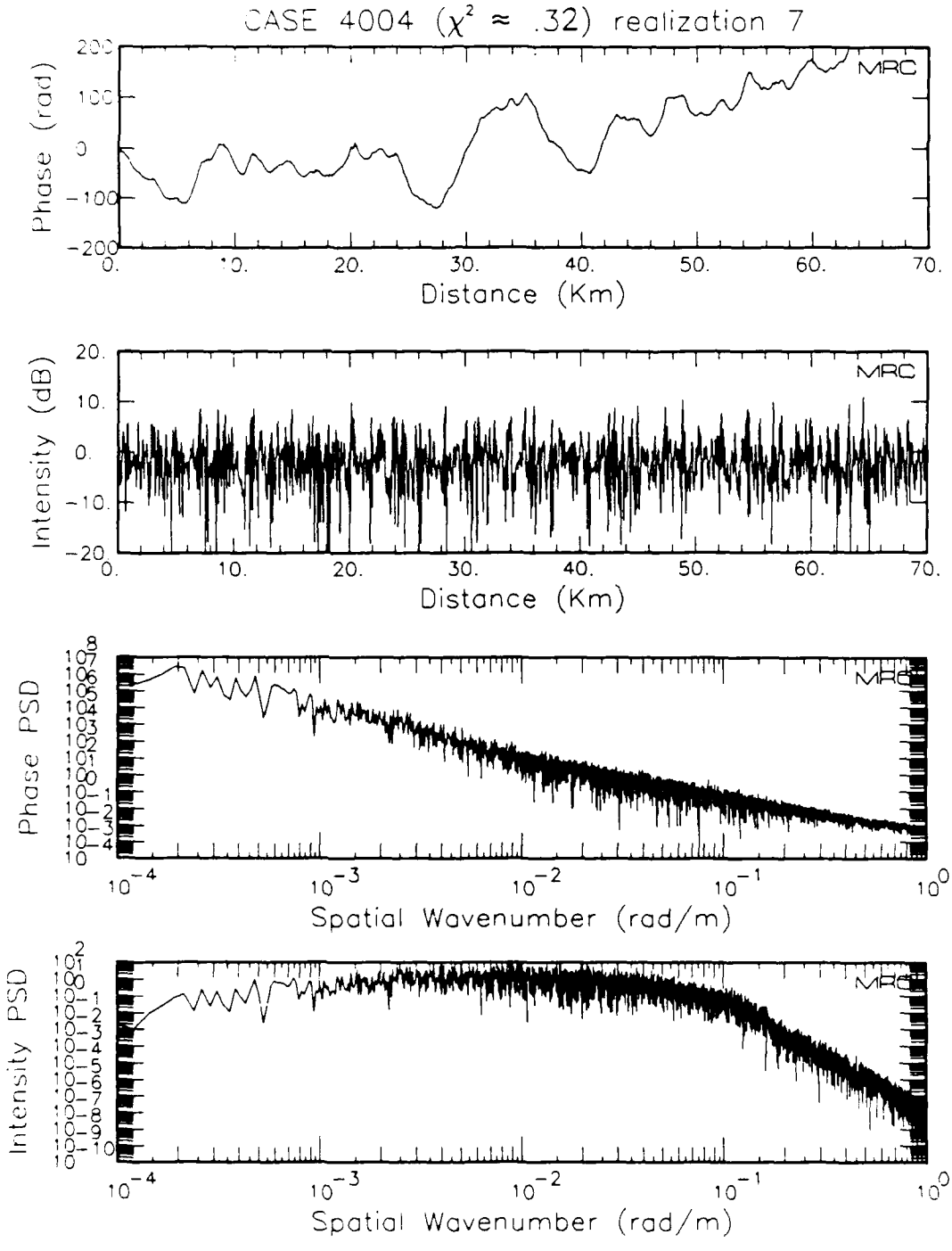

Figure 11. Representative phase, intensity, and power spectral density plots for case 4004.

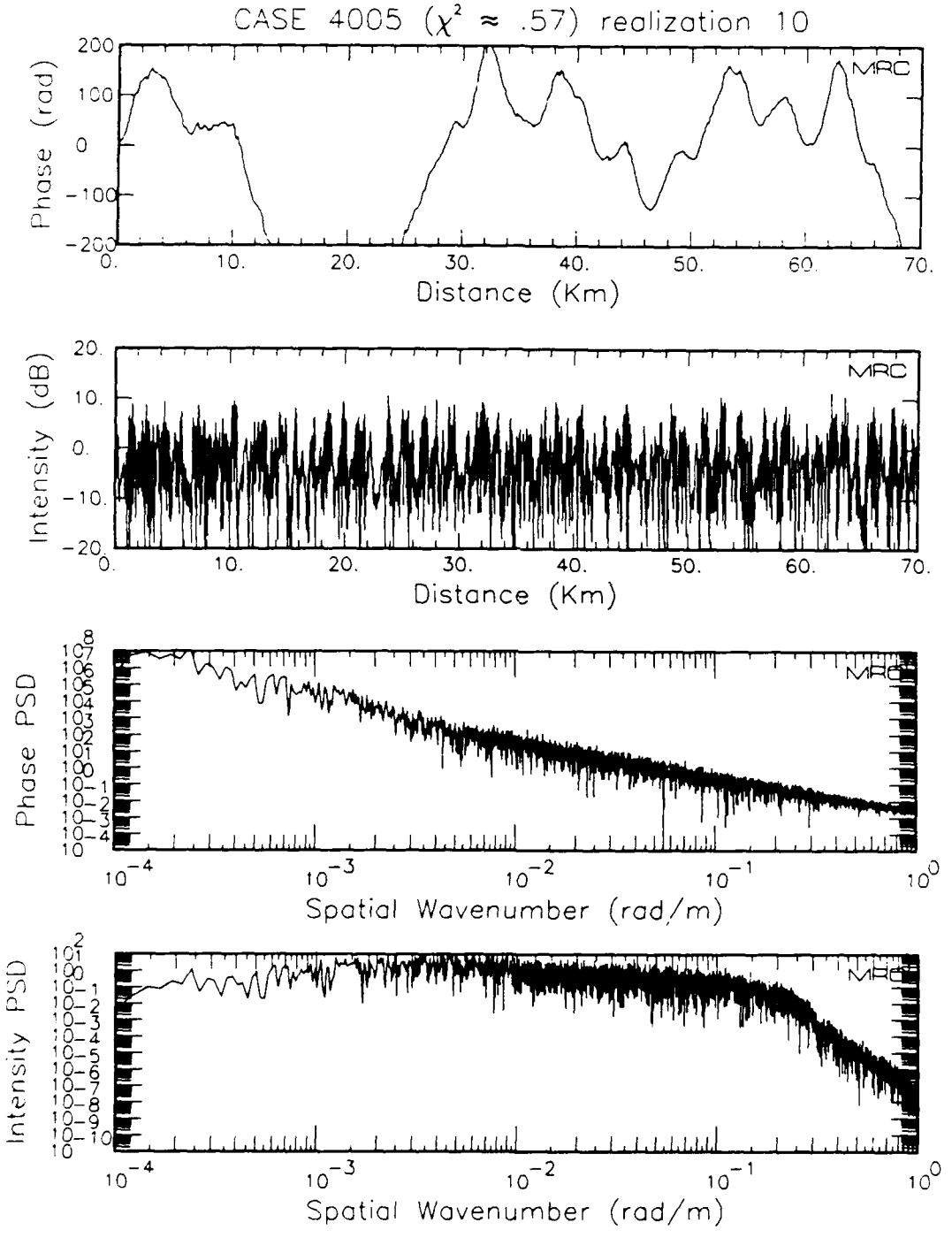

Figure 12. Representative phase, intensity, and power spectral density plots for case 4005.

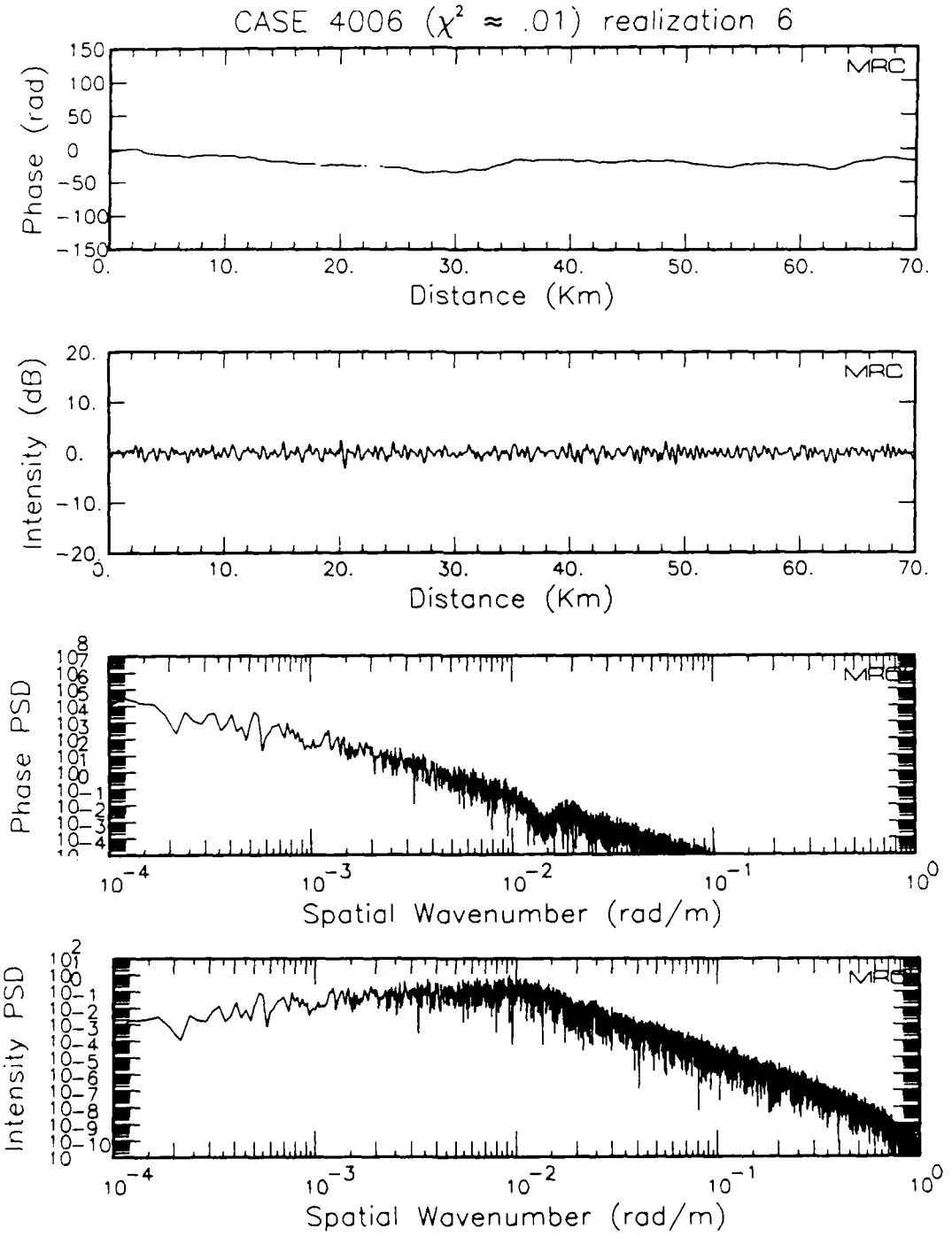

Figure 13. Representative phase, intensity, and power spectral density plots for case 4006.

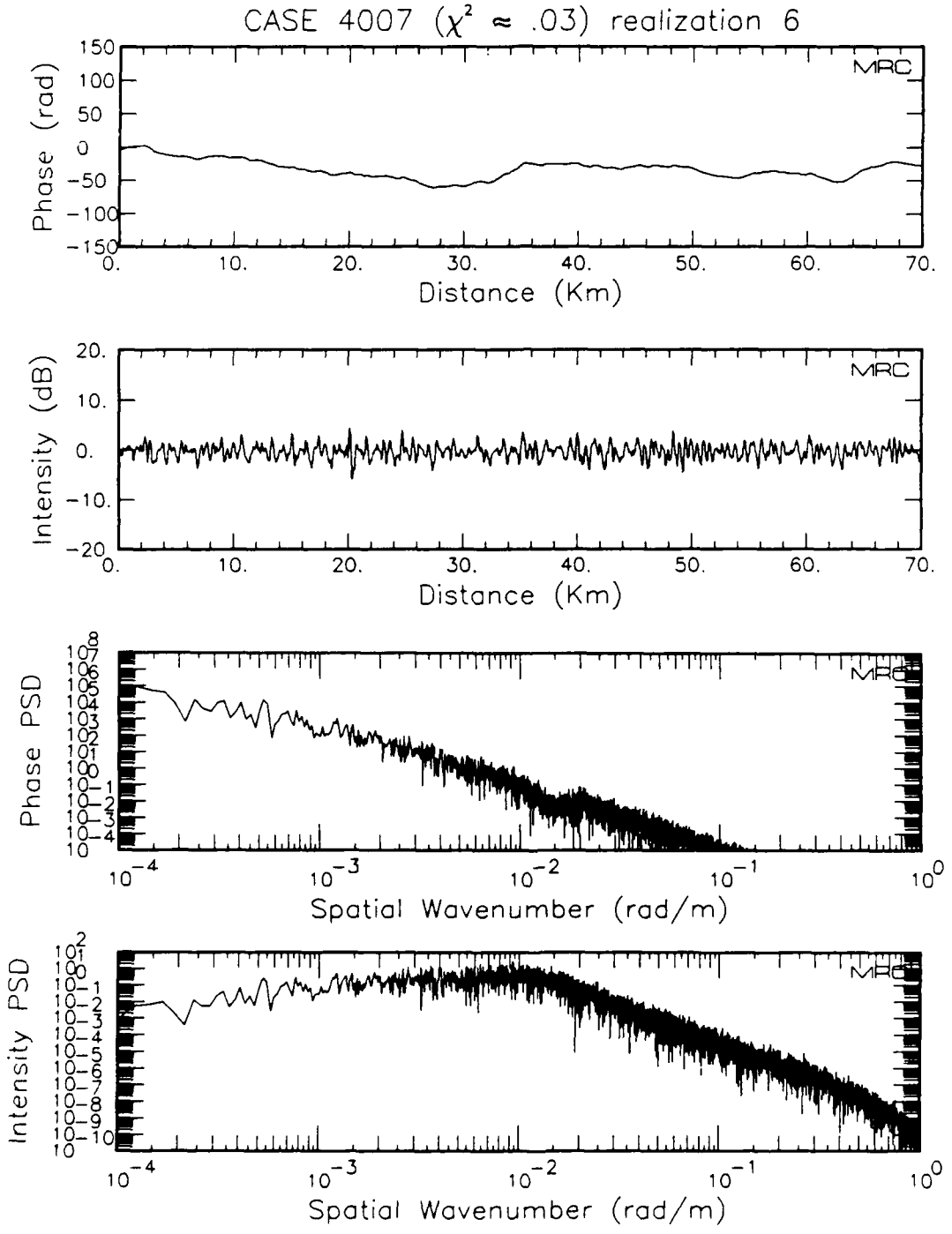

Figure 14. Representative phase, intensity, and power spectral density plots for case 4007.

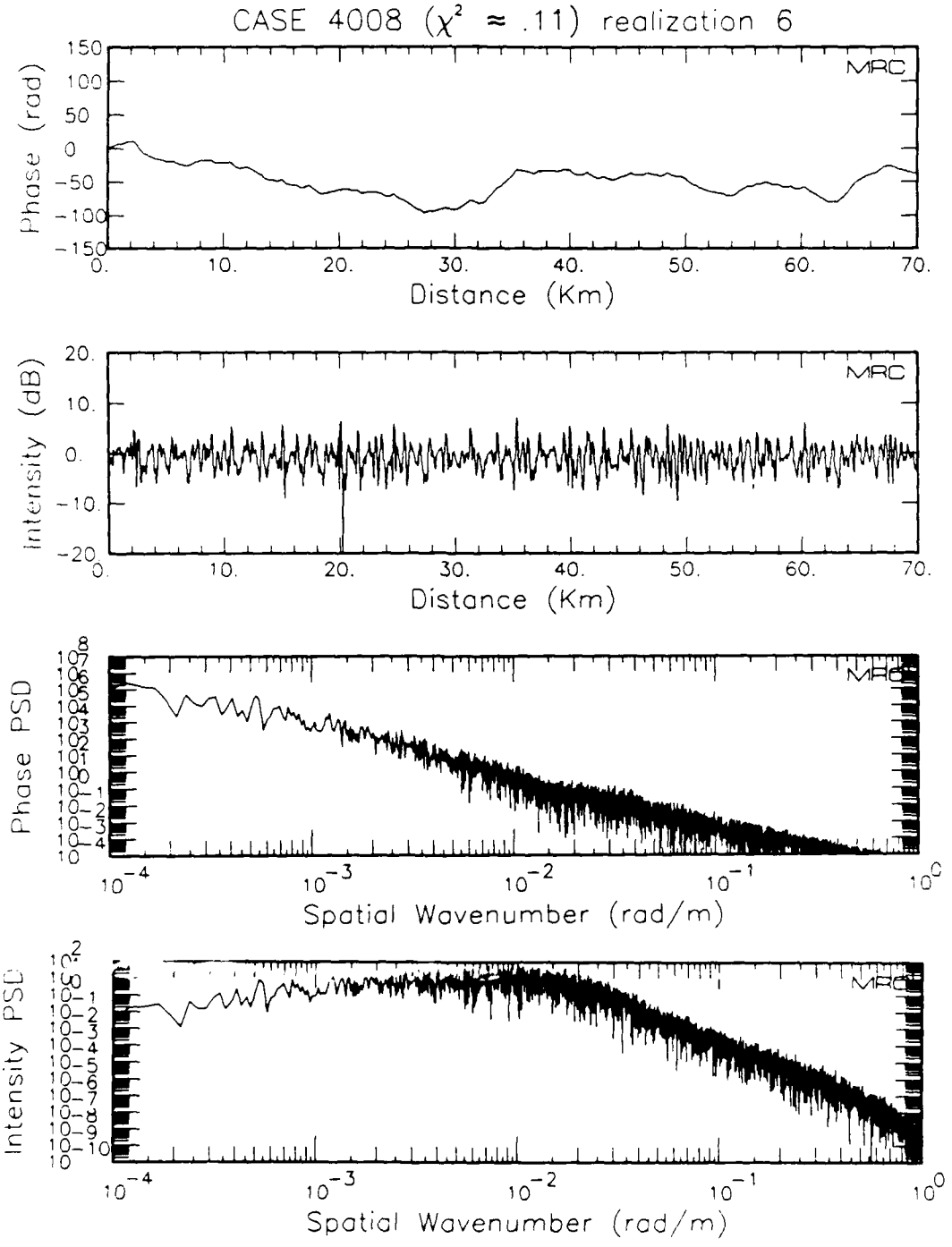

Figure 15. Representative phase, intensity, and power spectral density plots for case 4008.

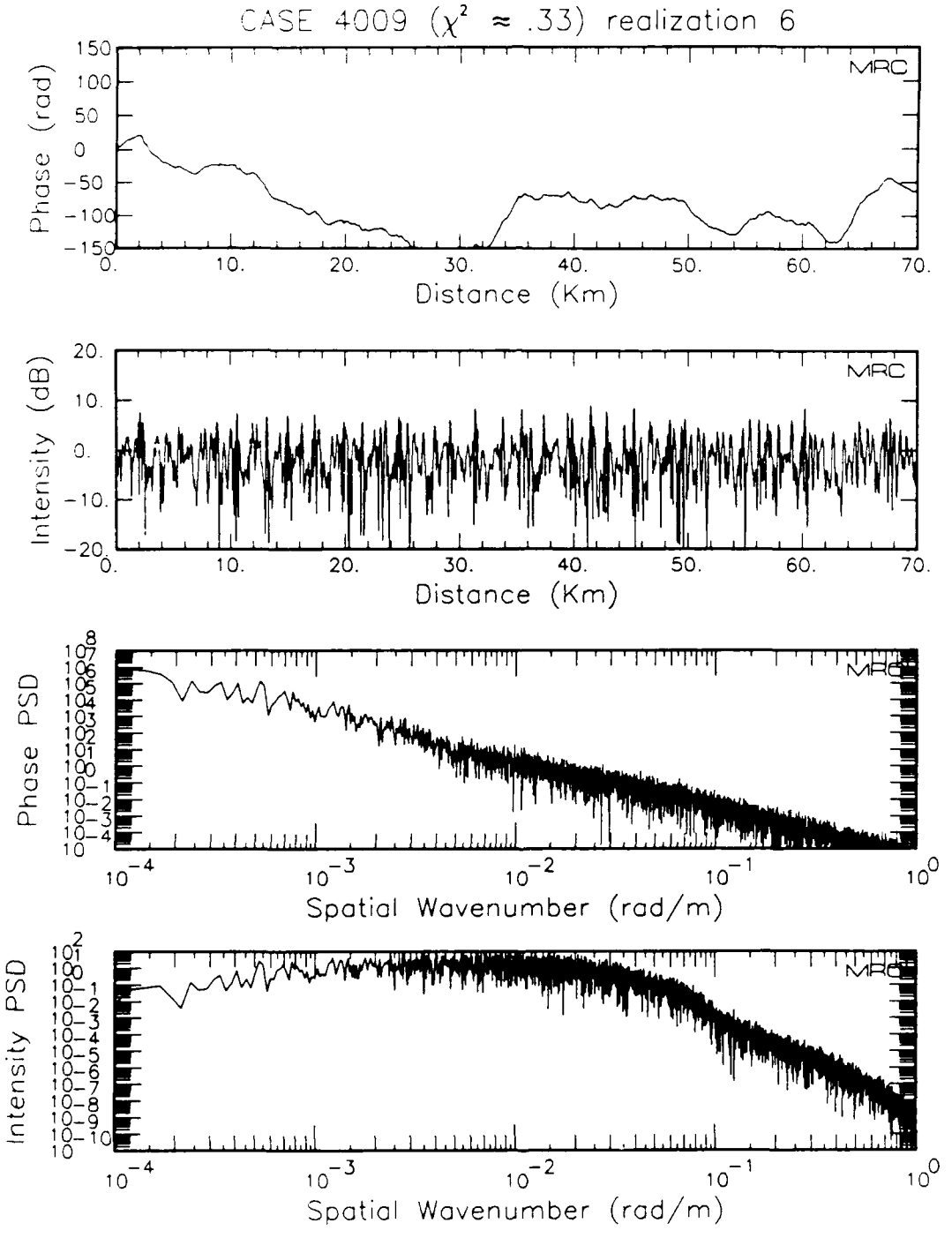

Figure 16. Representative phase, intensity, and power spectral density plots for case 4009.

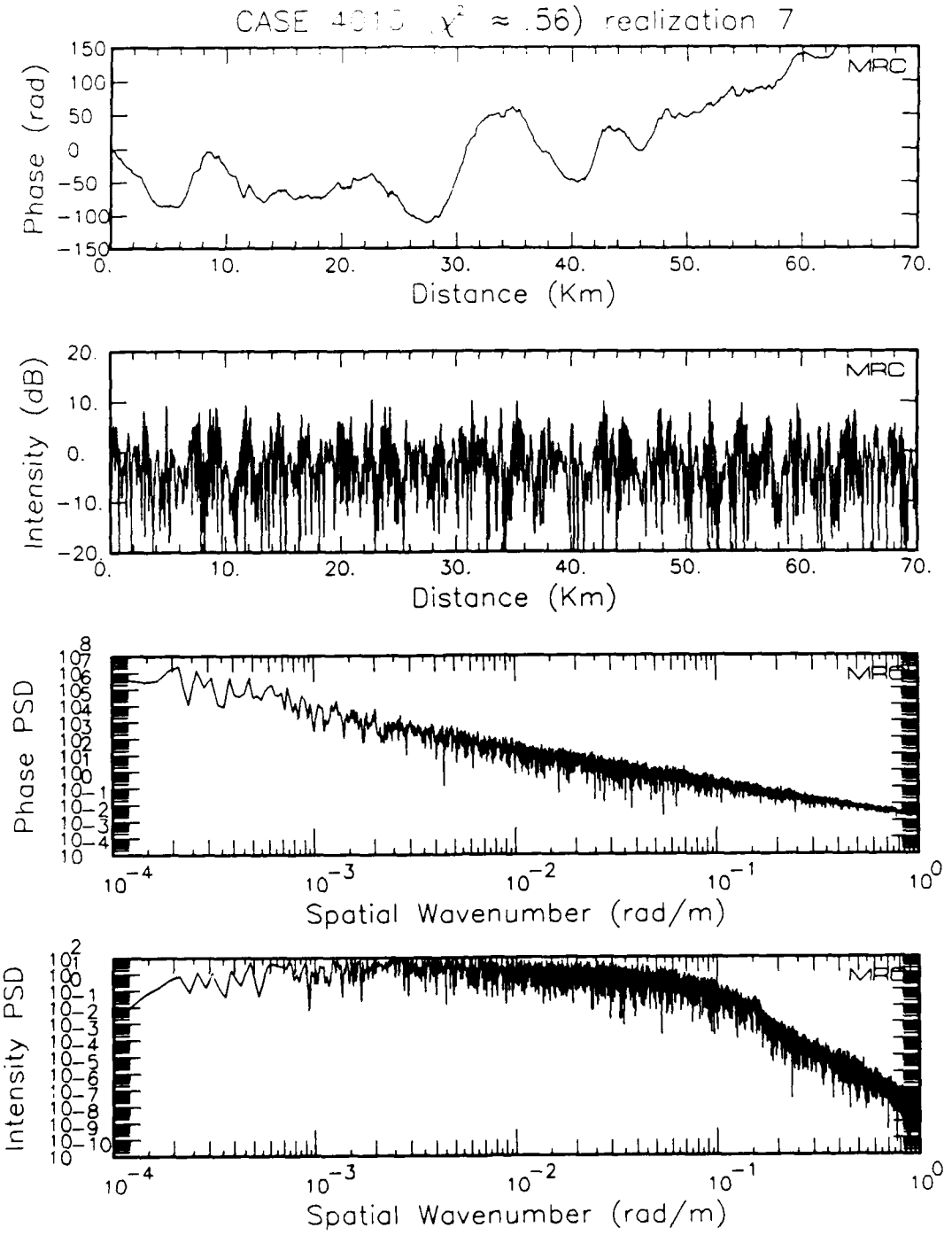

Figure 17. Representative phase, intensity, and power spectral density plots for case 4010.

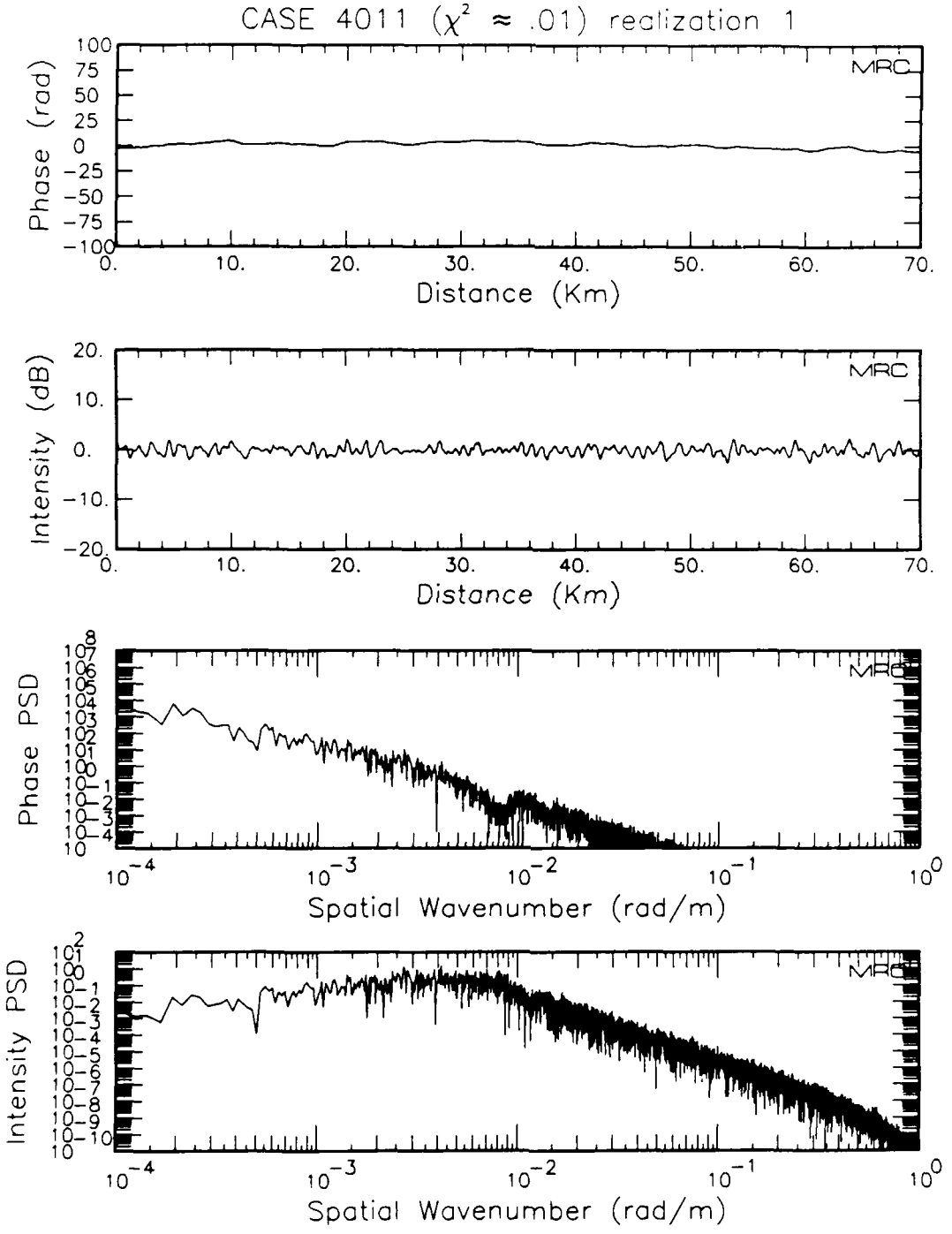

Figure 18. Representative phase, intensity, and power spectral density plots for case 4011.

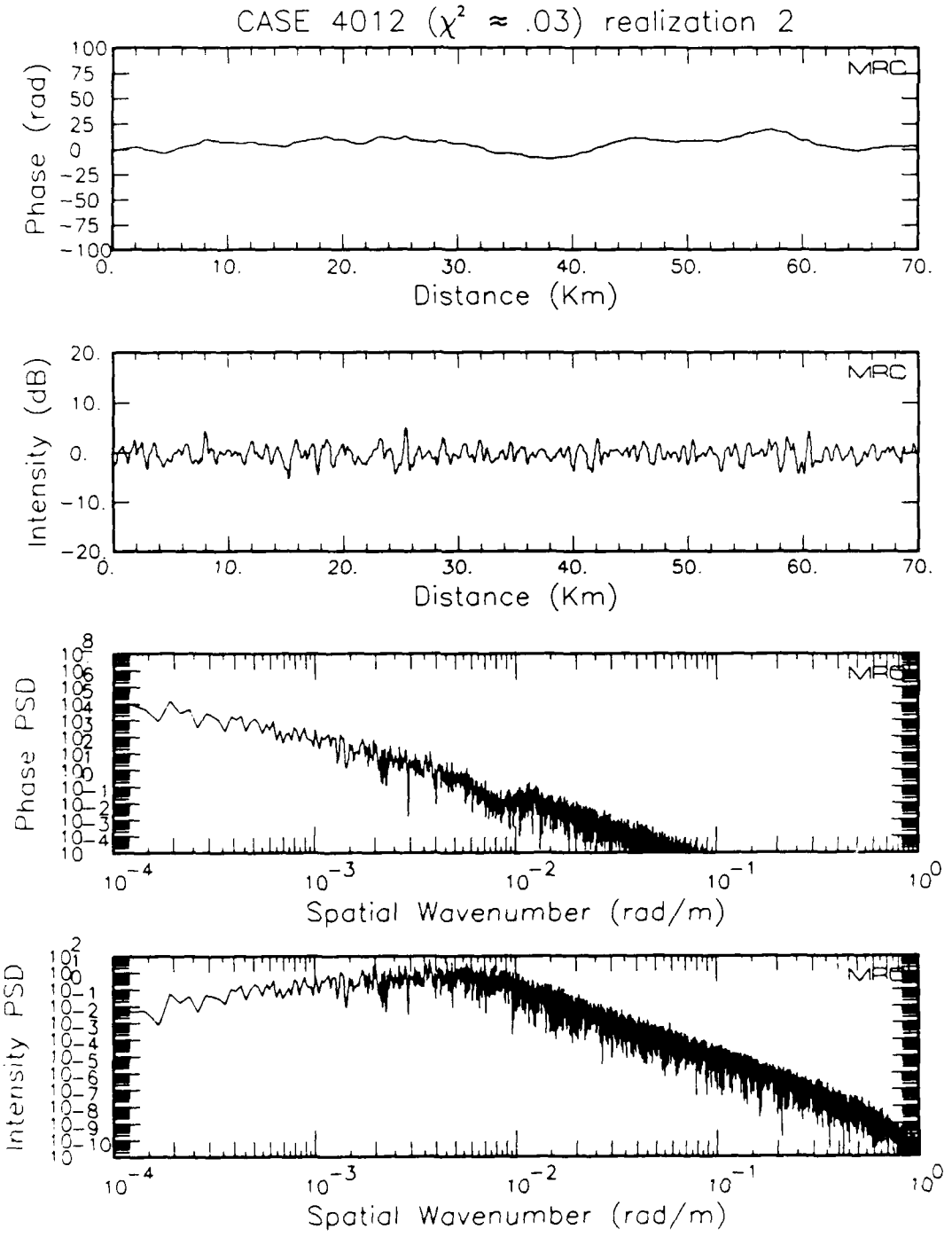

Figure 19. Representative phase, intensity, and power spectral density plots for case 4012.

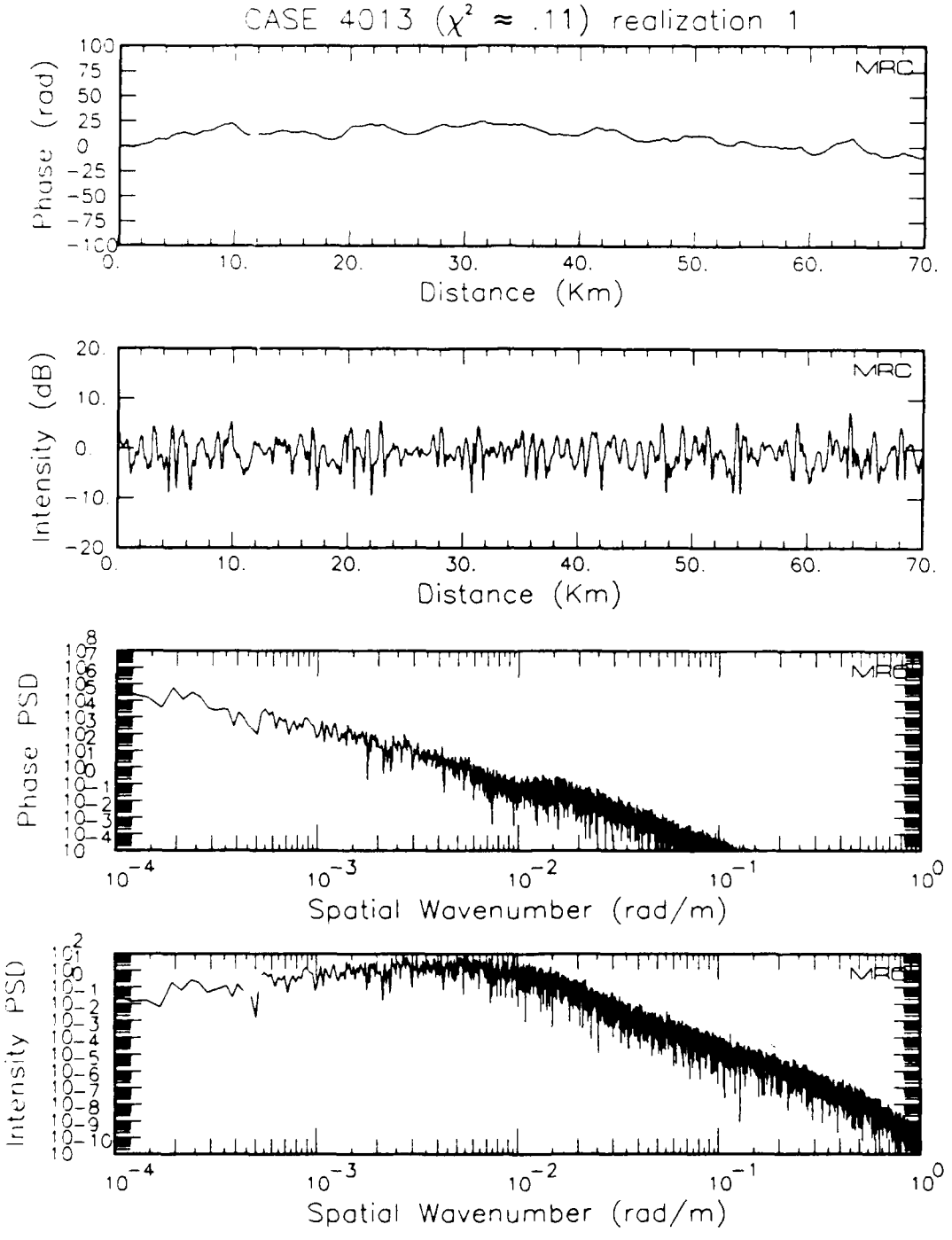

Figure 20. Representative phase, intensity, and power spectral density plots for case 4013.

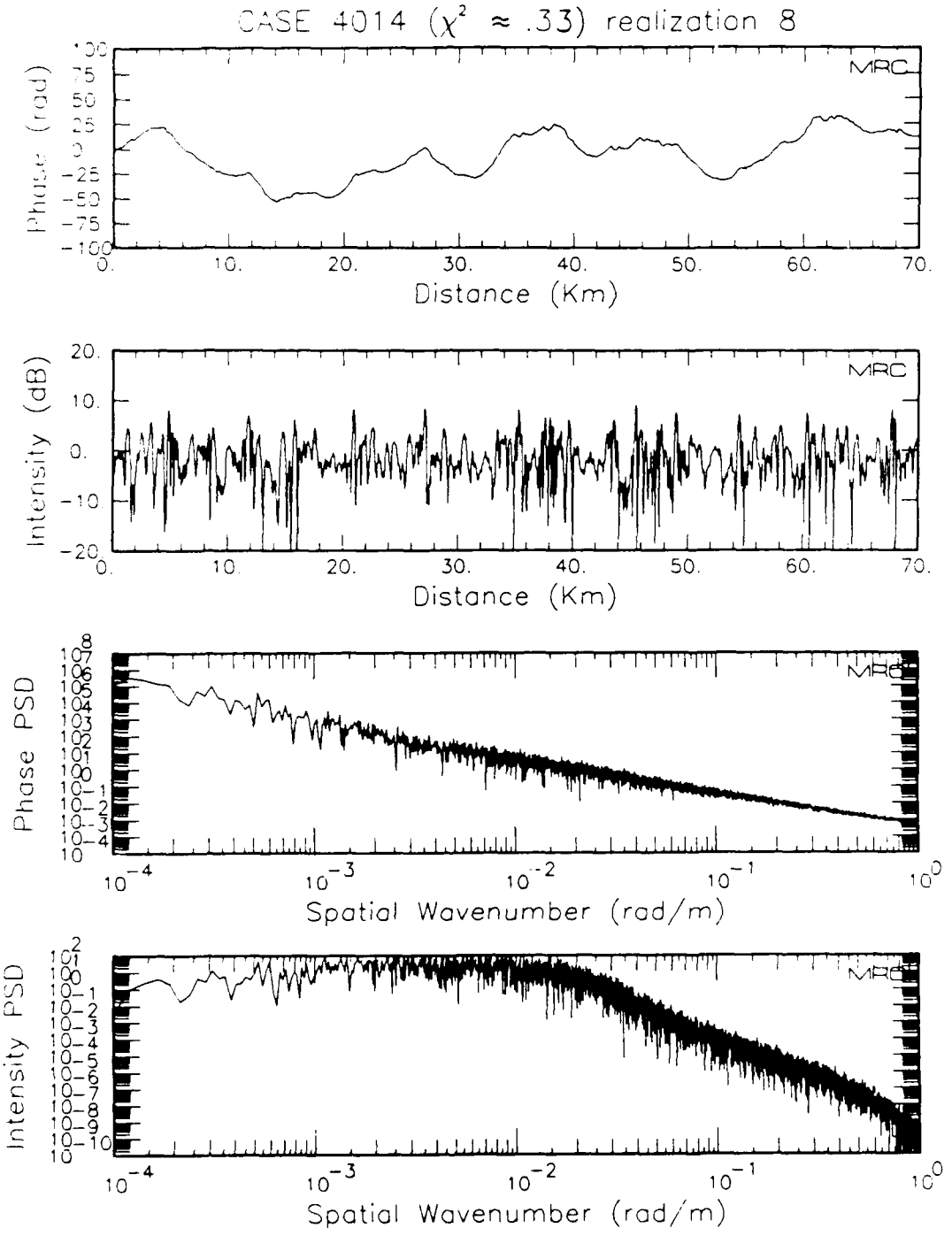

Figure 21. Representative phase, intensity, and power spectral density plots for case 4014.

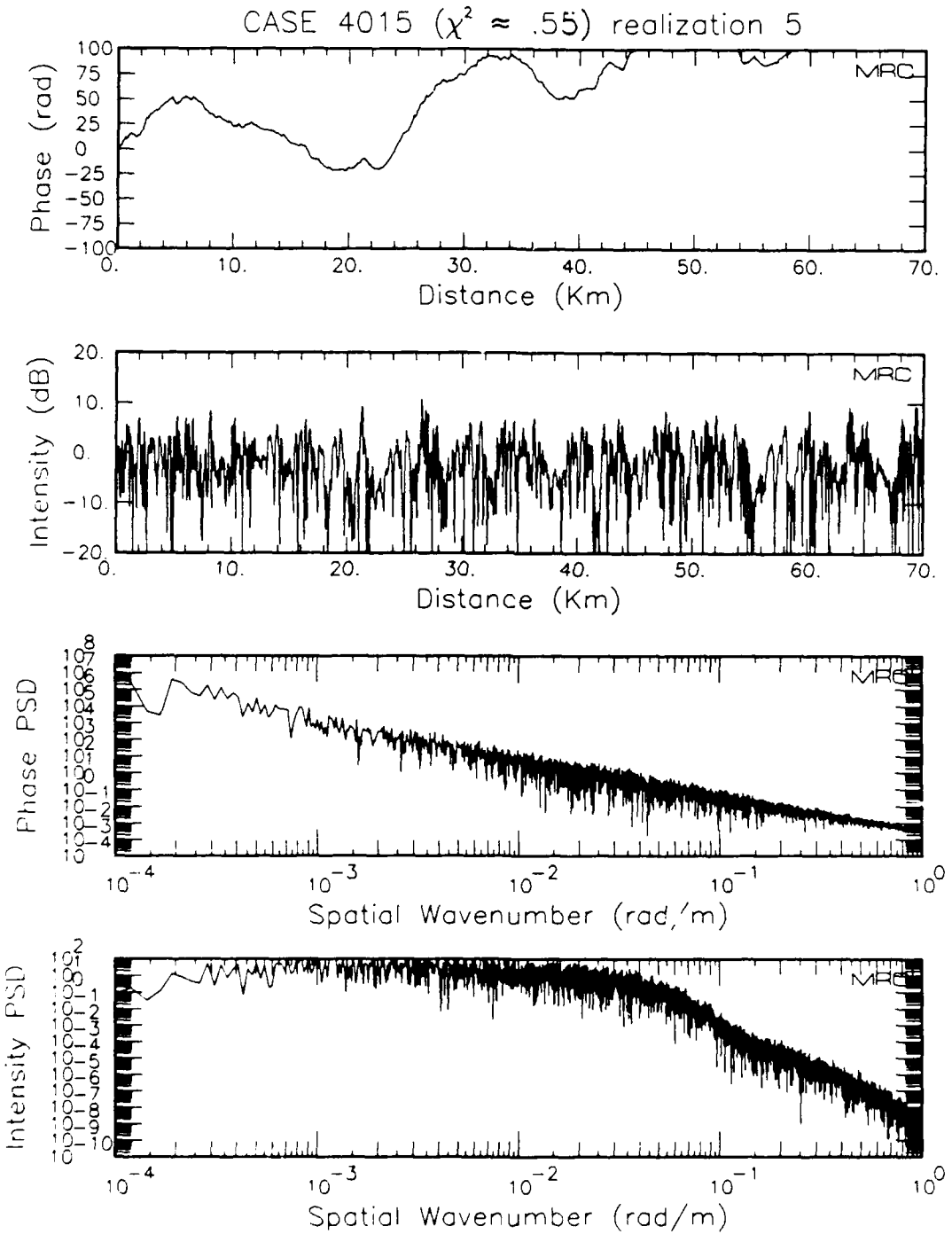

Figure 22. Representative phase, intensity, and power spectral density plots for case 4015.

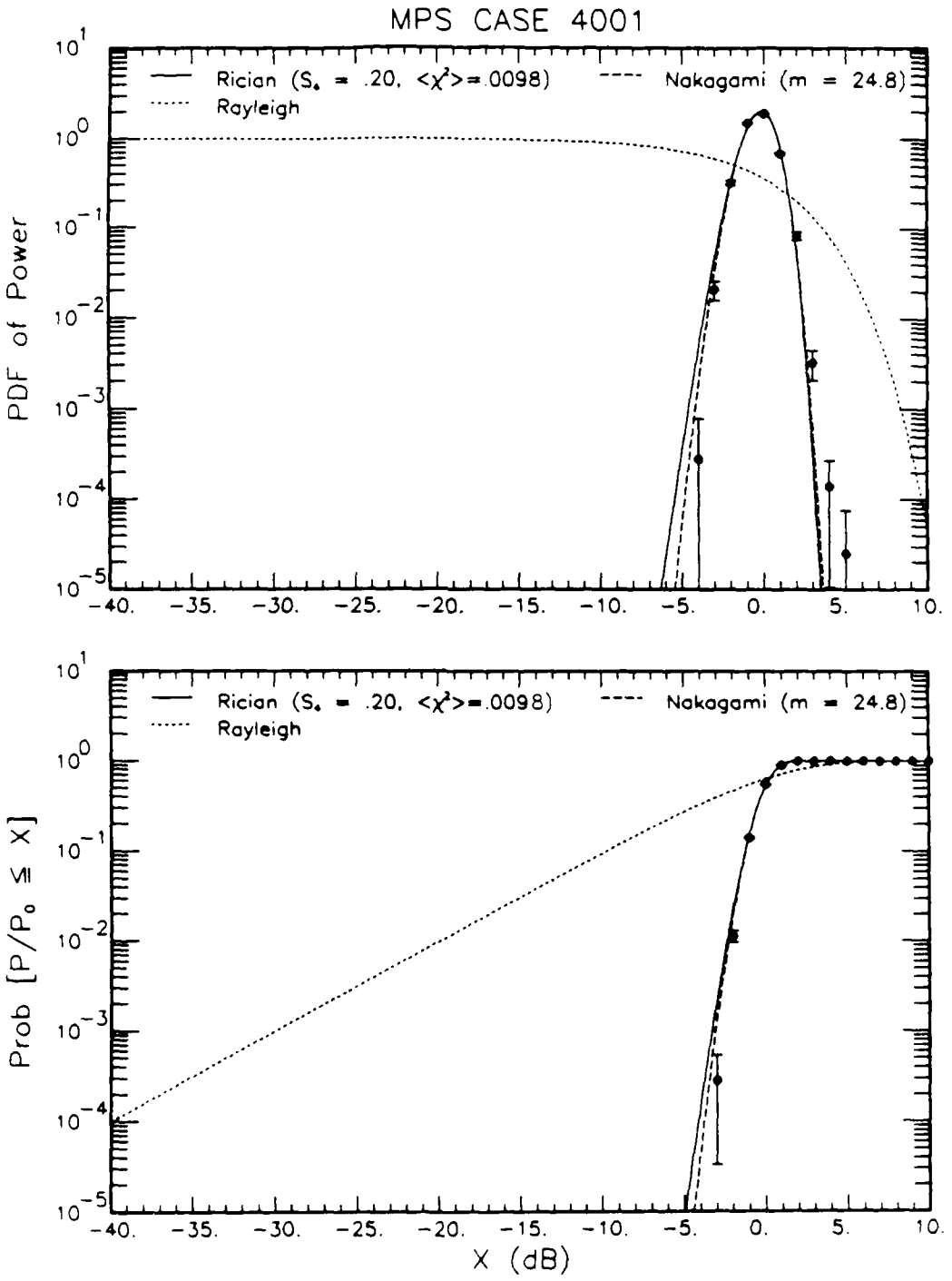

Figure 23. Comparison of Rayleigh, Rician, and Nakagami-m PDFs and CDFs for case 4001.

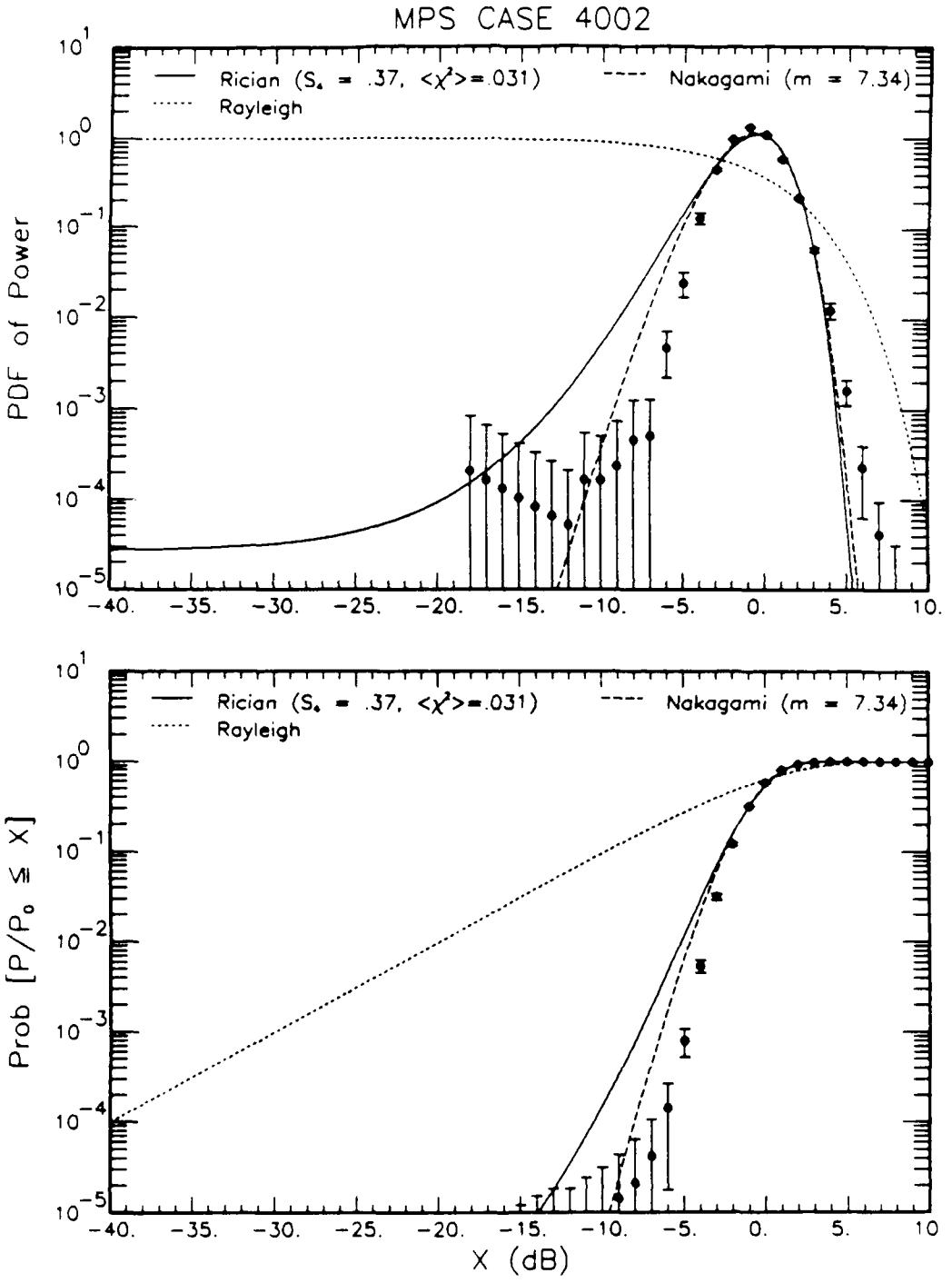

Figure 24. Comparison of Rayleigh, Rician, and Nakagami-m PDFs and CDFs for case 4002.

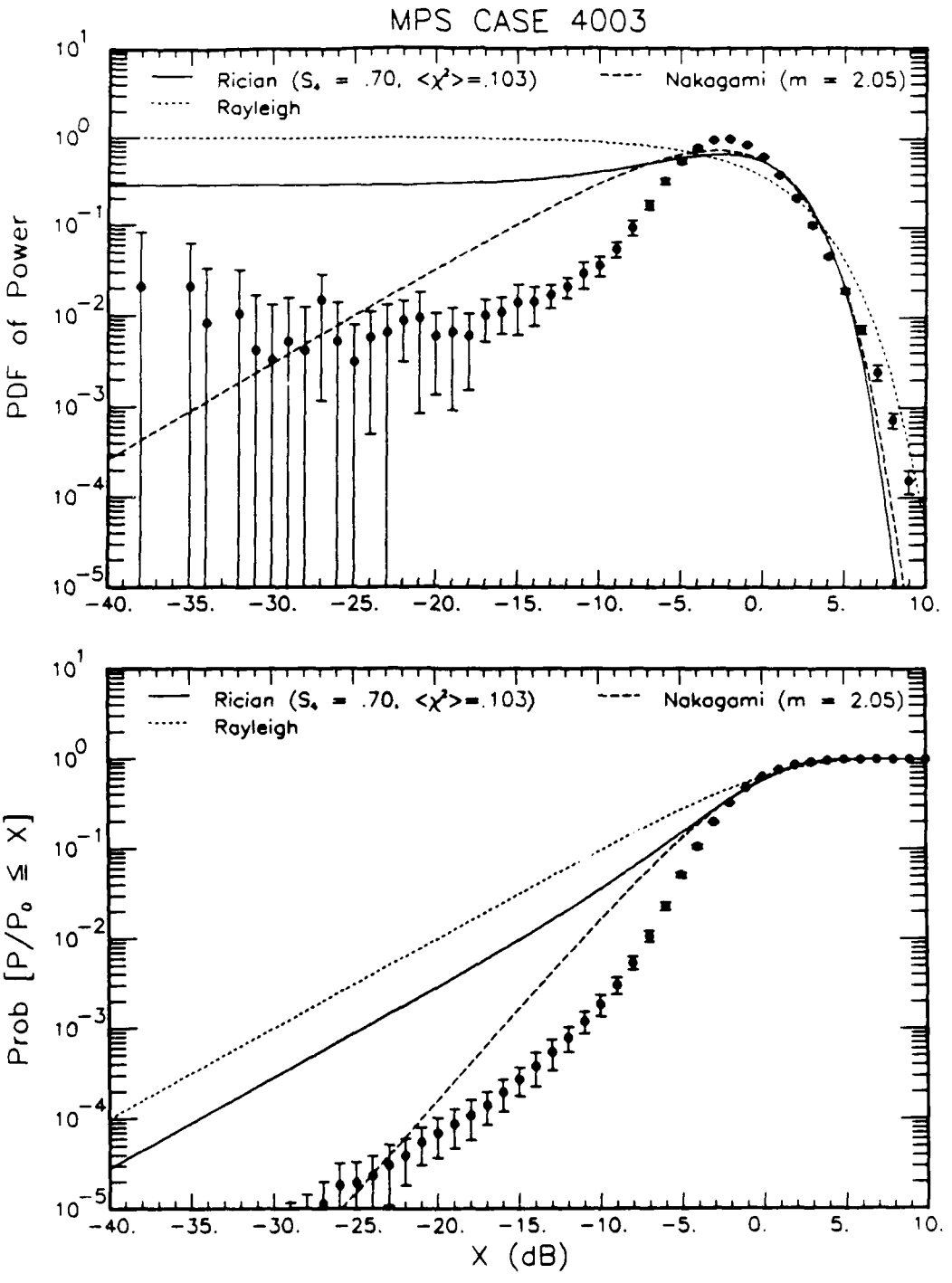

Figure 25. Comparison of Rayleigh, Rician, and Nakagami-m PDFs and CDFs for case 4003.

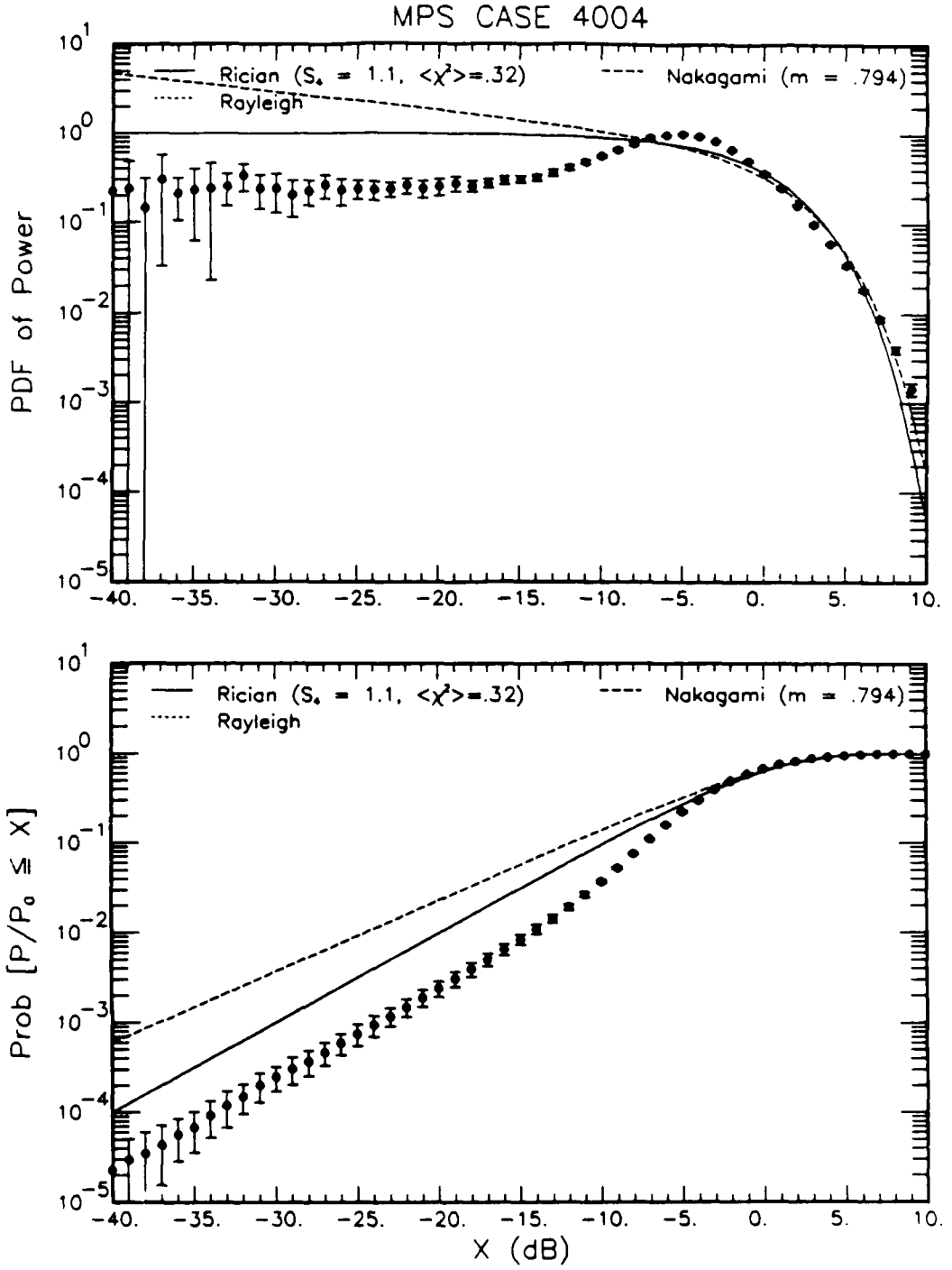

Figure 26. Comparison of Rayleigh, Rician, and Nakagami-m PDFs and CDFs for case 4004.

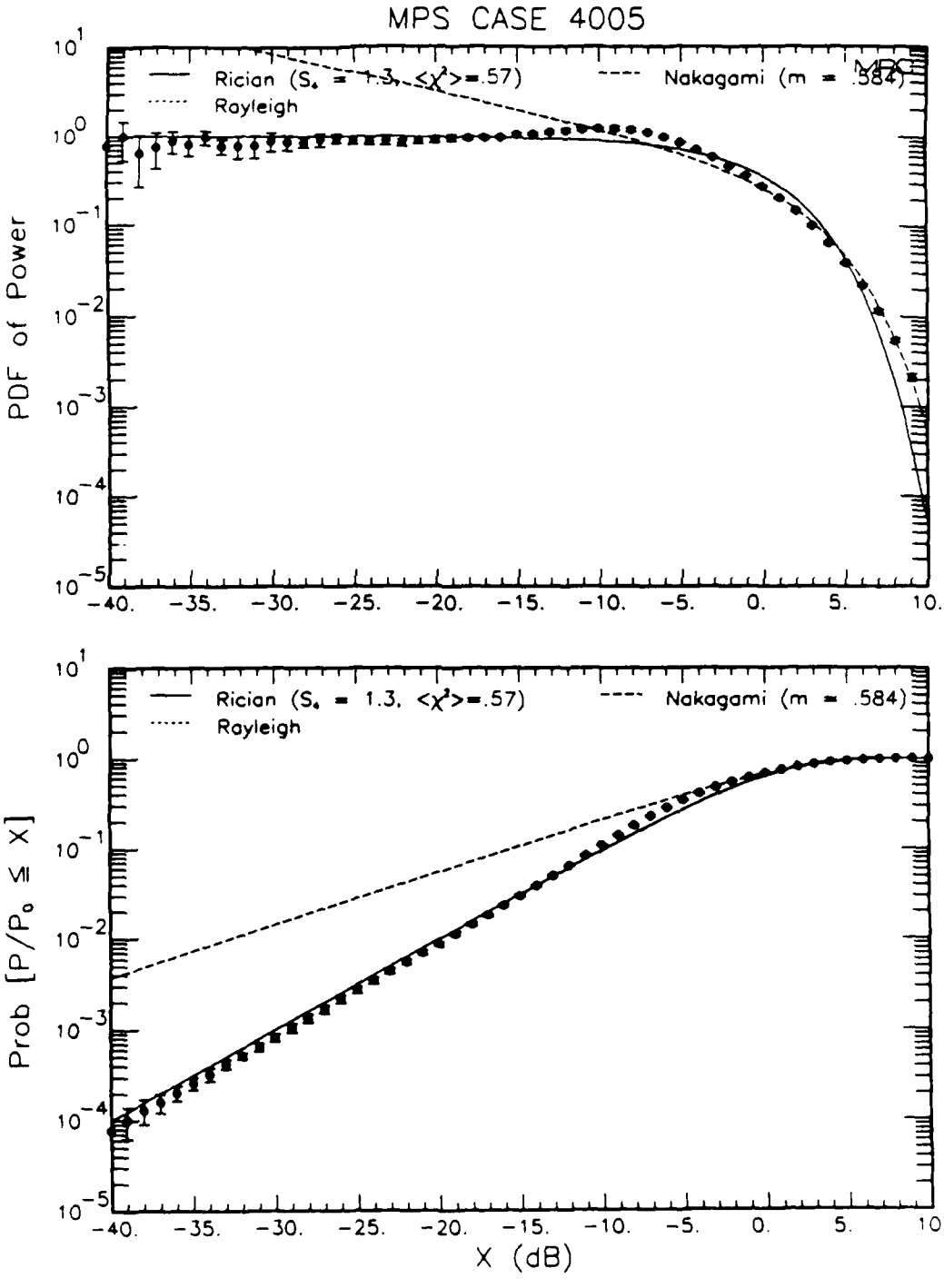

Figure 27. Comparison of Rayleigh, Rician, and Nakagami-m PDFs and CDFs for case 4005.

DISTRIBUTION LIST

DNA-TR-89-73

DEPARTMENT OF DEFENSE

US NUCLEAR COMMAND & CENTRAL SYST SUPPORT STAFF
ATTN: H SEQUINE

ASSISTANT TO THE SECRETARY OF DEFENSE ATOMIC ENERGY
ATTN: EXECUTIVE ASSISTANT

DEFENSE ADVANCED RSCH PROJ AGENCY
ATTN: DR MANSFIELD
ATTN: R ALEWINE

DEFENSE COMMUNICATIONS AGENCY
ATTN: A320

DEFENSE COMMUNICATIONS ENGINEER CENTER
ATTN: CODE R410

DEFENSE INTELLIGENCE AGENCY
ATTN: DC-6
ATTN: DIR
ATTN: DT-1B
ATTN: RTS-2B
ATTN: VP-TPO

DEFENSE NUCLEAR AGENCY
ATTN: DFSP G ULLRICH
ATTN: NANF
ATTN: NASF
ATTN: OPNA
3 CYS ATTN: RAAE
ATTN: RAAE A MARDIGUIAN
ATTN: RAAE G ULLRICH
ATTN: RAAE L SCHROCK
ATTN: RAAE M CRAWFORD
ATTN: RAAE P FLEMING
ATTN: RAAE S BERGGREN
ATTN: RAEE
4 CYS ATTN: TITL

DEFENSE NUCLEAR AGENCY
ATTN: TDNM
2 CYS ATTN: TDTT W SUMMA

DEFENSE TECHNICAL INFORMATION CENTER
2 CYS ATTN: DTIC/FDAB

JOINT DATA SYSTEM SUPPORT CTR
ATTN: R MASON

JOINT STRAT TGT PLANNING STAFF
ATTN: JK
ATTN: JKCS
ATTN: JLWT
ATTN: JPEM
ATTN: JPSS

NATIONAL SECURITY AGENCY
ATTN: C GOEDEKE

STRATEGIC AND THEATER NUCLEAR FORCES
ATTN: DR E SEVIN
ATTN: DR SCHNEITER
ATTN: LC R DAWSON

STRATEGIC DEFENSE INITIATIVE ORGANIZATION
ATTN: C GIESE
ATTN: K OBRIEN
ATTN: KE
ATTN: COL GUIBERSON
ATTN: W SEIBERLING
ATTN: SLKT
ATTN: SN
ATTN: COL R ROSS

THE JOINT STAFF
ATTN: J6

DEPARTMENT OF THE ARMY

ARMY LOGISTICS MANAGEMENT CTR
ATTN: DLSIE

DEP CH OF STAFF FOR OPS & PLANS
ATTN: DAMO-RQC

HARRY DIAMOND LABORATORIES
ATTN: SLCIS-IM-TL

U S ARMY ATMOSPHERIC SCIENCES LAB
ATTN: DR F NILES
ATTN: SLCAS-AE-E
ATTN: DR H HOLT

U S ARMY COMMUNICATIONS R&D COMMAND
ATTN: AMSEL-RD-ESA

U S ARMY FOREIGN SCIENCE & TECH CTR
ATTN: DRXST-SD

U S ARMY MISSILE COMMAND/AMSMI-RD-CS-R
ATTN: AMSMI-RD-CS-R

U S ARMY NUCLEAR & CHEMICAL AGENCY
ATTN: MONA-NU

U S ARMY NUCLEAR EFFECTS LABORATORY
ATTN: ATAA-PL
ATTN: ATAA-TDC
ATTN: ATRC-WCC

U S ARMY STRATEGIC DEFENSE CMD
ATTN: BMDSC-HI M POPE
ATTN: CSSD-H-TT M POPE
ATTN: R BRADSHAW
ATTN: R SMITH
ATTN: DASD-H-SAV

U S ARMY STRATEGIC DEFENSE COMMAND
ATTN: R W DICKERSON

USA SURVIVABILITY MANAGMENT OFFICE
ATTN: J BRAND

DEPARTMENT OF THE NAVY

COMMAND & CONTROL PROGRAMS
ATTN: OP 941

JOINT CRUISE MISSILES PROJECT OFC (PM-3)
ATTN: JCMG-707

NAVAL AIR SYSTEMS COMMAND
ATTN: PMA 271

NAVAL ELECTRONICS ENGRG ACTVY, PACIFIC
ATTN: D OBRYHIM

NAVAL RESEARCH LABORATORY
ATTN: J BROWN
ATTN: TECH LIB
2 CYS ATTN: H GUNSKY
ATTN: H HECKATHORN
ATTN: CODE 4183
ATTN: CODE 4701
ATTN: J DAVIS
ATTN: P RODRIGUEZ
ATTN: B RIPIN
ATTN: DR P BERNHARDT
ATTN: J HUBA
ATTN: CODE 5300
ATTN: M KAPLAN

NAVAL SURFACE WARFARE CENTER
ATTN: CODE H-21

NAVAL TECHNICAL INTELLIGENCE CTR
ATTN: DA41

NAVAL UNDERWATER SYSTEMS CENTER
ATTN: J KATAN

OFC OF THE DEPUTY CHIEF OF NAVAL OPS
ATTN: NOP 941D
ATTN: OP 654
ATTN: OP 981N

SPACE & NAVAL WARFARE SYSTEMS CMD
ATTN: T HUGHES
ATTN: PD 50TD
ATTN: G BRUNHART
ATTN: S KEARNEY
ATTN: F W DIEDERICH

THEATER NUCLEAR WARFARE PROGRAM OFC
ATTN: D SMITH

DEPARTMENT OF THE AIR FORCE

AIR FORCE CTR FOR STUDIES & ANALYSIS
ATTN: AFCSA/SASC

AIR FORCE ELECTRONIC WARFARE CENTER
ATTN: LT M MCNEELY

AIR FORCE SPACE SYSTEMS DIVISION
ATTN: CAPT T ABBOUSHI
ATTN: YA
2 CYS ATTN: YN

AIR UNIVERSITY LIBRARY
ATTN: AUL-LSE

BALLISTIC SYSTEMS DIVISION
ATTN: ENSE
ATTN: PK

HQ AWS, DET 3 (CSTC/WE)
ATTN: WE

SECRETARY OF AF/AQQS
ATTN: AF/RDQI

STRATEGIC AIR COMMAND/XRFS
ATTN: XRFS

WEAPONS LABORATORY
ATTN: NTCA
ATTN: NTN
ATTN: SUL

DEPARTMENT OF ENERGY

EG&G, INC
ATTN: D WRIGHT

LAWRENCE LIVERMORE NATIONAL LAB
ATTN: T DONICH

LOS ALAMOS NATIONAL LABORATORY
ATTN: D SAPPENFIELD
ATTN: D WINSKE
ATTN: J MALIK
ATTN: T KUNKLE

SANDIA NATIONAL LABORATORIES
ATTN: D HARTLEY

SANDIA NATIONAL LABORATORIES
ATTN: A D THORNBROUGH
ATTN: C S WILLIAMS
ATTN: R BACKSTROM
ATTN: D DAHLGREN
ATTN: C MEHL
ATTN: W D BROWN
ATTN: SPACE PROJECT DIV
ATTN: TECH LIB 3141

OTHER GOVERNMENT

CENTRAL INTELLIGENCE AGENCY
ATTN: OSWR/NED
ATTN: L BERG

DEPARTMENT OF COMMERCE
ATTN: C RUSH
ATTN: E MORRISON
ATTN: G REEVE
ATTN: J HOFFMEYER
ATTN: W UTLAUT

NATIONAL OCEANIC & ATMOSPHERIC ADMIN
ATTN: D WILLIAMS

U S DEPARTMENT OF STATE
ATTN: PM/TMP

DEPARTMENT OF DEFENSE CONTRACTORS

AEROSPACE CORP
ATTN: A LIGHTY
ATTN: A MORSE
ATTN: B P PURCELL
ATTN: C CREWS
ATTN: C RICE

ATTN: G LIGHT
ATTN: I GARFUNKEL
ATTN: J KLUCK
ATTN: M ROLENZ

ANALYTICAL SYSTEMS ENGINEERING CORP
ATTN: SECURITY

ATLANTIC RESEARCH SERVICES CORP
ATTN: R MCMILLAN

ATMOSPHERIC AND ENVIRONMENTAL RESEARCH INC
ATTN: M KO

AUSTIN RESEARCH ASSOCIATES
ATTN: J THOMPSON

AUTOMETRIC INCORPORATED
ATTN: C LUCAS

BDM INTERNATIONAL INC
ATTN: L JACOBS

BERKELEY RSCH ASSOCIATES, INC
ATTN: J WORKMAN
ATTN: S BRECHT

BOEING CO
ATTN: G HALL

CALIFORNIA RESEARCH & TECHNOLOGY, INC
ATTN: M ROSENBLATT

CHARLES STARK DRAPER LAB, INC
ATTN: A TETEWSKI

COMMUNICATIONS SATELLITE CORP
ATTN: G HYDE

CORNELL UNIVERSITY
ATTN: D FARLEY JR
ATTN: M KELLY

ELECTROSPACE SYSTEMS, INC
ATTN: P PHILLIPS

EOS TECHNOLOGIES, INC
ATTN: B GABBARD
ATTN: W LELEVIER

GENERAL ELECTRIC CO
ATTN: C ZIERDT
ATTN: R EDSALL

GENERAL RESEARCH CORP INC
ATTN: J EOLL

GRUMMAN AEROSPACE CORP
ATTN: J DIGLIO

HSS, INC
ATTN: D HANSEN

INFORMATION SCIENCE, INC
ATTN: W DUDZIAK

INSTITUTE FOR DEFENSE ANALYSES
ATTN: E BAUER
ATTN: H WOLFHARD

J S LEE ASSOCIATES INC
ATTN: DR J LEE

JAYCOR
ATTN: J SPERLING

JOHNS HOPKINS UNIVERSITY
ATTN: C MENG
ATTN: J D PHILLIPS
ATTN: R STOKES
ATTN: T EVANS

KAMAN SCIENCES CORP
ATTN: E CONRAD
ATTN: G DITTBERNER

KAMAN SCIENCES CORPORATION
ATTN: B GAMBILL
ATTN: DASIAC
ATTN: R RUTHERFORD

KAMAN SCIENCES CORPORATION
ATTN: DASIAC

LOCKHEED MISSILES & SPACE CO, INC
ATTN: J HENLEY
ATTN: J KUMER
ATTN: R SEARS

LOCKHEED MISSILES & SPACE CO, INC
ATTN: D KREJCI

LTV AEROSPACE & DEFENSE COMPANY
2 CYS ATTN: LIBRARY

M I T LINCOLN LAB
ATTN: D TOWLE
ATTN: I KUPIEC
ATTN: M LEE

MARTIN MARIETTA DENVER AEROSPACE
ATTN: H VON STRUVE III
ATTN: J BENNETT

MAXIM TECHNOLOGIES, INC
ATTN: B RIDGEWAY
ATTN: J SO

MCDONNELL DOUGLAS CORPORATION
ATTN: J GROSSMAN
ATTN: R HALPRIN

METATECH CORPORATION
ATTN: R SCHAEFER
ATTN: W RADASKY

METEOR COMMUNICATIONS CORP
ATTN: R LEADER

MISSION RESEARCH CORP
ATTN: R ARMSTRONG
ATTN: W WHITE

MISSION RESEARCH CORP
2 CYS ATTN: D KRUEGER
2 CYS ATTN: M DUFF
2 CYS ATTN: S FRASIER
ATTN: B R MILNER
ATTN: C LONGMIRE

ATTN: D ARCHER
ATTN: D KNEPP
ATTN: D LANDMAN
ATTN: F FAJEN
ATTN: F GUIGLIANO
ATTN: G MCCARTOR
ATTN: K COSNER
ATTN: M FIRESTONE
ATTN: R BIGONI
ATTN: R BOGUSCH
ATTN: R DANA
ATTN: R HENDRICK
ATTN: R KILB
ATTN: S GUTSCHE
ATTN: TECH INFO CENTER
ATTN: TECH LIBRARY

MITRE CORPORATION
ATTN: D RAMPTON

MITRE CORPORATION
ATTN: M HORROCKS
ATTN: R C PESCI
ATTN: W FOSTER

NORTHWEST RESEARCH ASSOC, INC
ATTN: E FREMOUW

PACIFIC SIERRA RESEARCH CORP
ATTN: E FIELD JR
ATTN: F THOMAS
ATTN: H BRODE

PHOTOMETRICS, INC
ATTN: I L KOFSKY

PHOTON RESEARCH ASSOCIATES
ATTN: D BURWELL
ATTN: O LEWIS

PHYSICAL RESEARCH INC
ATTN: W SHIH

PHYSICAL RESEARCH INC
ATTN: H FITZ
ATTN: P LUNN

PHYSICAL RESEARCH, INC
ATTN: R DELIBERIS
ATTN: T STEPHENS

PHYSICAL RESEARCH, INC
ATTN: J DEVORE
ATTN: J THOMPSON
ATTN: W SCHLUETER

R & D ASSOCIATES
ATTN: C GREIFINGER
ATTN: F GILMORE
ATTN: G HOYT
ATTN: M GANTSWEG

RAND CORP
ATTN: C CRAIN
ATTN: E BEDROZIAN

RAND CORP
ATTN: B BENNETT

RJO ENTERPRISES/POET FAC
ATTN: A ALEXANDER
ATTN: W BURNS

SCIENCE APPLICATIONS INTL CORP
ATTN: S ROSENCWEIG

SCIENCE APPLICATIONS INTL CORP
ATTN: C SMITH
ATTN: D HAMLIN
ATTN: D SACHS
ATTN: E STRAKER
ATTN: L LINSON

SCIENCE APPLICATIONS INTL CORP
ATTN: D TELAGE
ATTN: M CROSS

SRI INTERNATIONAL
ATTN: J DEPP
ATTN: R LEONARD
ATTN: W CHESNUT
ATTN: W JAYE

STEWART RADIANCE LABORATORY
ATTN: R HUPPI

TELECOMMUNICATION SCIENCE ASSOCIATES
ATTN: R BUCKNER

TELEDYNE BROWN ENGINEERING
ATTN: J WOLFSBERGER, JR
ATTN: N PASSINO

TOYON RESEARCH CORP
ATTN: J ISE

TRW INC
ATTN: R PLEBUCH
ATTN: H CULVER

TRW SPACE & DEFENSE SYSTEMS
ATTN: D M LAYTON

USER SYSTEMS, INC
ATTN: S W MCCANDLESS, JR

UTAH STATE UNIVERSITY
ATTN: K BAKER
ATTN: L JENSEN

VISIDYNE, INC
ATTN: J CARPENTER